Article:
Pabois, O, Ziolek, RM, Lorenz, CD et al. (2021) Morphology of bile salts micelles and mixed micelles with lipolysis products, from scattering techniques and atomistic simulations. Journal of Colloid and Interface Science, 587. pp. 522-537. ISSN: 0021-9797

https://doi.org/10.1016/j.jcis.2020.10.101

Morphology of bile salts micelles and mixed micelles with lipolysis products, from scattering techniques and atomistic simulations

Olivia Pabois[a, b], Robert M. Ziolek[c], Christian D. Lorenz[c], Sylvain Prévost[a], Najet Mahmoudi[d], Maximilian W. A. Skoda[d], Rebecca J. L. Welbourn[d], Margarita Valero[e], Richard D. Harvey[f], Myriam M.-L. Grundy[g], Peter J. Wilde[h], Isabelle Grillo[a], Yuri Gerelli[a, i*], Cécile A. Dreiss[b*]

[a] Institut Laue-Langevin, Grenoble 38000, France

[b] Institute of Pharmaceutical Science, King's College London, London SE1 9NH, United Kingdom

[c] Department of Physics, King's College London, London WC2R 2LS, United Kingdom

[d] ISIS, Science and Technology Facilities Council, Rutherford Appleton Laboratory, Didcot OX11 0QX, United Kingdom

[e] Department of Physical Chemistry, University of Salamanca, Salamanca 37007, Spain

[f] Department of Pharmaceutical Chemistry, University of Vienna, Vienna A-1090, Austria

[g] PEGASE, INRAE, Institut Agro, Saint Gilles 35590, France

[h] Quadram Institute Bioscience, Norwich Research Park, Norwich NR4 7UQ, United Kingdom

[i] Department of Life and Environmental Sciences, Polytechnic University of Marche, Ancona 60131, Italy

E-mail addresses:

olivia.pabois@kcl.ac.uk; rob.ziolek@kcl.ac.uk; chris.lorenz@kcl.ac.uk; prevost@ill.fr; najet.mahmoudi@stfc.ac.uk; maximilian.skoda@stfc.ac.uk; becky.welbourn@stfc.ac.uk; mvalero@usal.es; richard.harvey@univie.ac.at; myriam.grundy@inrae.fr; peter.wilde@quadram.ac.uk; y.gerelli@univpm.it; cecile.dreiss@kcl.ac.uk

Corresponding authors:

Cécile A. Dreiss:

King's College London

School of Cancer & Pharmaceutical Sciences

Franklin-Wilkins Building

150 Stamford Street

SE1 9NH London, UK

Tel: +44 (0)207 848 3766

Yuri Gerelli:

Polytechnic University of Marche

Department of Life and Environmental Sciences

6, via Brecce Bianche

60131 Ancona, Italy

Tel: +39 071 220 4608

Abstract

Hypotheses. Bile salts (BS) are biosurfactants released into the small intestine, which play key and contrasting roles in lipid digestion: they adsorb at interfaces and promote the adsorption of digestive enzymes onto fat droplets, while they also remove lipolysis products from that interface, solubilising them into mixed micelles. Small architectural variations on their chemical structure, specifically their bile acid moiety, are hypothesised to underlie these conflicting functionalities, which should be reflected in different aggregation and solubilisation behaviour.

Experiments. The micellisation of two BS, sodium taurocholate (NaTC) and sodium taurodeoxycholate (NaTDC), which differ by one hydroxyl group on the bile acid moiety, was assessed by pyrene fluorescence spectroscopy, and the morphology of aggregates formed in the absence and presence of fatty acids (FA) and monoacylglycerols (MAG) – typical lipolysis products – were resolved by small-angle X-ray/neutron scattering (SAXS, SANS) and molecular dynamics simulations. The solubilisation by BS of triacylglycerol-incorporating liposomes – mimicking ingested lipids – was studied by neutron reflectometry and SANS.

Findings. Our results demonstrate that BS micelles exhibit an ellipsoidal shape. NaTDC displays a lower critical micellar concentration and forms larger and more spherical aggregates than NaTC. Similar observations were made for BS micelles mixed with FA and MAG. Structural studies with liposomes show that the addition of BS induces their solubilisation into mixed micelles, with NaTDC displaying a higher solubilising capacity.

Keywords

Bile salts; lipid digestion; bulk aggregation properties; lipolysis products; liposomes; small-angle scattering

Graphical abstract

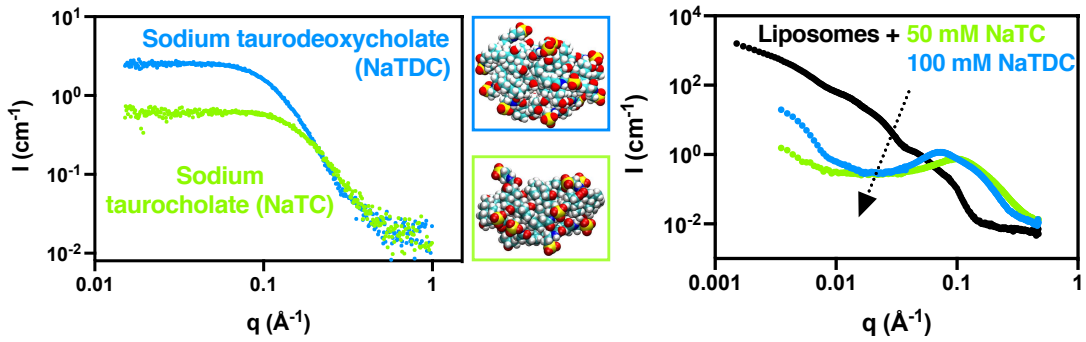

Bile salts molecular structure has an impact on their aggregation and solubilisation behaviours

Introduction

Understanding the process of lipid digestion, specifically, elucidating the origin of the contrasting roles of bile salts (BS) in this process, is critical towards developing new food formulations regulating calorie uptake, and addressing the current obesity crisis. The prevalence of obesity worldwide has nearly tripled since 1975, and currently at least 2.8 million people die each year as a result of being either overweight or obese [1].

BS are biosurfactants produced in the liver, stored in the gall bladder and secreted into the duodenum (small intestine) [2], which carry out two fundamental functions in fat (lipid) digestion and absorption [3,4]. Firstly, they promote enzyme binding to the lipid droplet/water interface, thus allowing enzyme-catalysed lipolysis [5–8]; secondly, they promote the desorption of enzyme-inhibiting insoluble lipolysis products (diacylglycerols (DAG), monoacylglycerols (MAG) and free fatty acids (FFA)) accumulating at the interface, by incorporating them into mixed micelles and transporting them to the gut mucosa for absorption [2,9,10], in addition to effectively displacing food-stabilising proteins adsorbed on fat droplets surfaces [11,12]. While the role of BS on lipid digestion and absorption is indisputable, their mechanism of action still needs to be unlocked. Recent investigations carried out at the air/water interface, either bare [13,14] or stabilised by a phospholipid [14] or a polysaccharide [15] film, and on a hydrophobic surface [16] have suggested that BS distinct functions during lipolysis arise from their architectural diversity, in particular the very small variations (i.e., the position and number of hydroxyl groups) on their bile acid portion. Characterising BS behaviour in solution and the impact of their molecular structure is therefore key to establishing the source of their different functionalities in the gut.

BS are unconventional surface-active materials made up of a short and flexible ionic chain linked to a rigid and slightly curved steroid skeleton (the hydrophobic “tail”), which contains weakly separated hydrophilic (hydroxyl groups) and hydrophobic (methyl groups) faces [17]. This unusual planar polarity enables them to self-assemble in solution into micelles, whose mechanism of formation and structure are still under debate, despite extensive investigations [18,19]. Two models, both involving the hydrophobic effect and intermolecular hydrogen bonding, have been proposed to describe their self-organisation process: (i) a two-step mechanism, whereby primary, small micelles form, and subsequently associate with each other into secondary, larger micelles [20,21]; (ii) a continuous self-association process,

following which aggregates grow in size upon the addition of unimers [22,23]. These models result in various shapes and sizes for BS micelles, from globular [23–29] and rod-like [24,30–34], to disc-shaped [35] and helical [36–38] structures. These discrepancies across the existing body of literature call for further structural characterisations to provide a clear molecular-level picture of BS complex aggregates and thus better understand BS physicochemical properties and biological roles.

BS are also known to solubilise molecules formed during the lipolysis process in the small intestine: the products of phospholipid, galactolipid and triacylglycerol (TAG) hydrolysis, such as MAG and FFA. These mixtures give rise to a range of phases, depending on the composition of the lipid/BS/water systems [39–41]. In this study, the area of interest is the region of high-water content, which reflects the actual duodenal composition, where lipids and BS are highly diluted in the gastrointestinal tract. While the phase diagram of some highly hydrated lipid/BS system has been established [42–44], showing the presence of mixed vesicles, mixed micelles and the coexistence of both phases [40,45,46], the dependence of the mechanism of vesicle/micelle transition on BS type and concentration, and the effect of temperature, remain largely unknown. A range of structural studies have been carried out mainly with the aim of assessing the effect of dilution on lipid/BS mixed micelles and demonstrated a micelle-to-vesicle transition, driven by the differences in the solubility and spontaneous curvature of BS and lipids [47–50]. Upon dilution, BS molecules tend to leave the lipid/BS mixed micelles to maintain their bulk unimer concentration; since lipids display a lower spontaneous curvature than BS, the resulting increase in lipid/BS molar ratio in the micelles has been subsequently shown to induce a globular-to-cylindrical shape transition in a range of lipid/BS mixtures. Based on small-angle neutron scattering (SANS) measurements, a common cylindrical structure has been suggested for the aggregates of the lipophilic components (such as phospholipids [51] and MAG [50]), with the lipids being inserted radially and the BS lying flat between the lipid head groups, with their hydrophilic part facing the aqueous solvent. In lecithin/BS systems for instance, SANS data suggest that BS are mainly located in the end caps of the cylinder [52]. As soon as the amount of BS molecules is no longer sufficient to maintain the cylindrical body, the mixed aggregates transform into BS-incorporating lipid vesicles. The same effect (i.e., micelle elongation, followed by vesicle formation) is observed upon increasing the lipid/BS molar ratio [53]. Some work has also been reported on the vesicle-to-micelle reverse pathway occurring upon solubilisation of lipid

vesicles into mixed micelles by BS, which we examine in this study, and the same (but reverse) sequence of structures was observed upon addition of increasing amounts of BS to liposomes [42,54–56]. This ability of BS to induce micellar solubilisation, which is a crucial step in the transportation of nutrients towards the gut mucosa, where they are absorbed [9], arises from their amphiphilic character. While the transitions between these different aggregate structures have been reported, there is still a lack of structural studies, in particular on the impact of BS structural diversity, their localisation in the aggregates and their lipid-solubilisation capacity.

This work reports a structural investigation of the micellisation of two selected BS, sodium taurocholate (NaTC) and sodium taurodeoxycholate (NaTDC) (Figure 1), on their own, and in the presence of typical products of TAG lipolysis, namely: fatty acids (FA) and monoacylglycerols (MAG). These two BS were selected because they are known to exhibit contrasting adsorption/desorption dynamics at interfaces, possibly holding a key to their contrasting roles in lipid digestion [14,15], a hypothesis we explore here by focusing on the bulk aggregation behaviour. Following the structural characterisation of BS neat and mixed micelles, we investigate the outcome of their interaction with lipid vesicles, made up of 1,2-dipalmitoyl-*sn*-glycero-3-phosphocholine (DPPC) (Figure S1A) and TAG (the major type of dietary fats). Liposomes are used here as a mimic of colloidal structures found in the gastrointestinal tract, in order to compare the solubilising capacity of the two BS, which builds on our previous interfacial studies with monolayers of DPPC [14]. We employ an array of complementary techniques to examine the morphology of BS neat and mixed micelles: small-angle neutron and X-ray scattering (SANS, SAXS), neutron reflectometry (NR) and atomistic molecular dynamics (MD) simulations. In this study, caprylic (C8:0) and oleic (C18:1) acids were employed as FA, monocaprylin (C8:0) and monoolein (C18:1) as MAG, and tricaprylin (C8:0) and triolein (C18:1) as TAG (Figure S2), to evaluate the effect of both chain length and saturation on the structures formed.

Experimental section

Materials

NaTC (P97.0% TLC) (Figure 1), NaTDC (P95.0% TLC) (Figure 1), pyrene (puriss. p.a., for fluorescence, P99.0% GC), caprylic acid (C8:0 FA, P99.0%) (Figure S2), oleic acid (C18:1 FA, P99.0% GC) (Figure S2), monocaprylin (C8:0 MAG, P99.0%) (Figure S2), monoolein (C18:1 MAG, P99.0%) (Figure S2), sodium chloride (NaCl, P99.8%), tricaprylin (C8:0 TAG, P99.0%) (Figure S2), triolein (C18:1 TAG, P99.0%) (Figure S2), ethanol (EtOH, P99.8% GC) and acetone (AcOH, P99.5%) were all purchased from Sigma-Aldrich (Gillingham, UK). DPPC (Figure S1A) and 1,2-dipalmitoyl-d_{62}-*sn*-glycero-3-phosphocholine (d_{62}-DPPC) (Figure S1B) were purchased from Avanti Polar Lipids, Inc. (Alabaster, AL, USA), and chloroform ($CHCl_3$) from Fisher Scientific (Loughborough, UK). Ultrapure water, or MilliQ-grade water (H_2O, 18.2 MΩ·cm, Merck Millipore, Molsheim, France), was used in all experiments, except for the SANS measurements, where deuterium oxide (D_2O, P99.9%), provided by Euriso-top SAS (St. Aubin, France), was employed, and for NR experiments, where both D_2O and silicon-matched water (SiMW, 38% D_2O / 62% H_2O by volume) were used. All reagents were used as supplied.

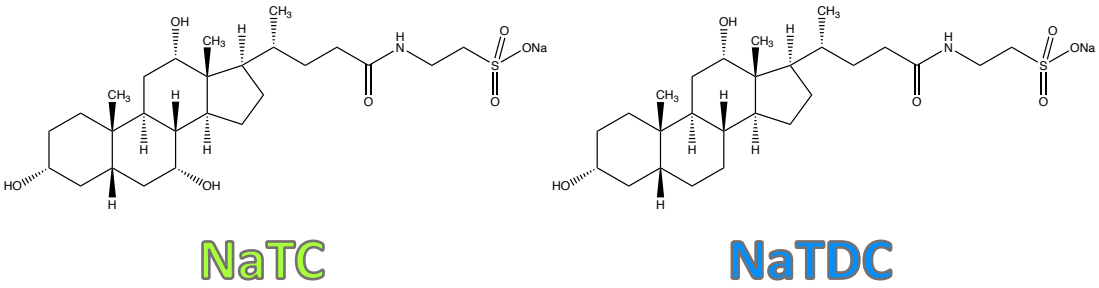

Figure 1: Structures of sodium taurocholate (NaTC) and sodium taurodeoxycholate (NaTDC). The same colour-coding for the two BS is used in some of the figures.

Methods

1. Pyrene fluorescence spectroscopy

The critical micellar concentrations (CMC) of NaTC and NaTDC were determined by fluorescence spectroscopy, using pyrene as a probe. This method is based on the dependence of pyrene fluorescence intensity on the environment polarity [57]. In the absence of micelles (below the CMC), pyrene is surrounded by polar molecules of water and the ratio of the third

to the first vibrational peaks (F_{III}/F_I, with $F_{III}/F_I = I_{III}/I_I$, where I_I and I_{III} are the intensities at wavelengths of 373 and 383 nm, respectively) is low. Above the CMC, pyrene partitions into the micelles and F_{III}/F_I increases because of the less polar environment.

Pyrene fluorescence emission (0.5 μM of pyrene in solutions of BS) was measured on a Cary Eclipse fluorescence spectrophotometer (Agilent Technologies UK Ltd, Stockport, UK), using 114F-QS quartz cells (Hellma Analytics, Müllheim, Germany), with excitation at 310 nm, both at 23 and 37°C. The F_{III}/F_I intensity ratio was fitted using the following equation:

$$F_{III}/F_I = F_0 + \frac{\mathrm{K}.\ \Delta F_{max}}{\mathrm{K}.\ \mathrm{e}^{-[BS].\ \mathrm{c}.\ \Delta F_{max}}} \quad (1)$$

where F_0 is the fluorescence emission intensity of pyrene in water, F_{max} the maximum fluorescence emission intensity of pyrene in the micellar aggregates, $\Delta F_{max} = F_{max} - F_0$ the maximum change in F_{III}/F_I, and K and c two constants [58]. F_0 and F_{max} were determined experimentally. ΔF_{max} characterises the polarity of the environment probed by pyrene: the higher this parameter, the higher the hydrophobicity. The fluorescence from BS was subtracted from the measurements. The CMC is taken here as the concentration value at which F_{III}/F_I starts to level off.

2. Neutron reflectometry

Neutron reflectometry (NR) measurements were performed on the INTER time-of-flight neutron reflectometer at ISIS pulsed neutron source (STFC Rutherford Appleton Laboratory, Didcot, UK) [59]. Details of the instrument configuration are provided in Supporting Information and sample preparation in this section.

DPPC/TAG liposomes preparation. Chain-deuterated lipids (d_{62}-DPPC) were dissolved in $CHCl_3$, with or without C8:0 (tricaprylin) or C18:1 (triolein) TAG. The organic solvent was then removed by using a rotavapor (at 474 mPa, at 40°C) and placing the samples under vacuum overnight (at 10 mPa, at 50°C). The solubility limit of each TAG in DPPC vesicles is around 14% for tricaprylin [60,61] and 3% for triolein [60,62,63]; therefore, TAG concentrations of, respectively, 12% and 2% (slightly below the threshold values) were employed. The dried lipid film was dispersed into degassed D_2O at a DPPC concentration of 2 mg/mL, and then vortex-mixed for 15 minutes. Thereafter, the hydrated lipid suspension was subjected to 5 cycles of 3-minute freezing (in liquid nitrogen) and 3-minute thawing, before tip-sonicating the

aqueous solution at a frequency of 20 kHz and amplitude of 30% (alternating between 2 seconds of pulse and 3 seconds of pause) for 30 minutes (SONOPULS HD 3100 ultrasonic homogeniser, microtip model: MS 73, BANDELIN electronic GmbH & Co. KG, Berlin, Germany), and centrifuging it at 11,000 rpm for 30 minutes, to remove titanium fragments. The liposome dispersion was finally extruded 11 times through 50 nm-pore size polycarbonate membranes (Avanti Mini-Extruder, Avanti Polar Lipids, Inc., Alabaster, AL, USA). The hydration and extrusion procedures were carried out at 50°C ± 2, well above the temperature of the main gel-to-fluid phase transition of d_{62}-DPPC ($T_{d62\text{-}DPPC\ phase\ transition} \approx 37°C$, which is around 3°C lower than $T_{DPPC\ phase\ transition}$) [64,65]. The phase transition temperatures of tricaprylin-incorporating (DPPC/TC) and triolein-incorporating (DPPC/TO) DPPC vesicles were preliminarily determined by micro-differential scanning calorimetry and were found to be lower than for DPPC ($T_{DPPC/TC\ phase\ transition} = 38.0 \pm 1.0°C$ and $T_{DPPC/TO\ phase\ transition} = 39.4 \pm 0.3°C$ *vs.* $T_{DPPC\ phase\ transition} = 40.2 \pm 0.4°C$) (Figure S3).

Solid-supported lipid bilayer (SLB) formation. Lipid bilayers were deposited onto silicon substrates (80 x 50 cm^2 surface) that were previously enclosed in laminar flow solid/liquid cells. The protocol for the deposition of SLB by vesicle fusion was defined with a quartz-crystal microbalance with dissipation monitoring (more detail in Supporting Information, Figure S4). Prior to any measurement, the flow cells were thoroughly cleaned through bath sonication in EtOH, and the silicon blocks in $CHCl_3$, AcOH and EtOH, sequentially, before rinsing both extensively with ultrapure water and drying them under nitrogen. The silicon substrates were then treated by UV/Ozone to further remove organic impurities and have more hydrophilic surfaces. Once assembled, the cells were prefilled with degassed D_2O for alignment and pre-characterisation purposes. The solid/liquid cells were connected to a liquid chromatography pump, which allowed for easy exchange of the buffer solutions.

Liposomes were injected by hand into the flow cells at a temperature of 50°C ± 2 (well above $T_{d62\text{-}DPPC\ phase\ transition} \approx 37°C$ [64,65]). Salt (0.5 M NaCl) was then flushed into the solid/liquid cells, to induce, by osmotic shock, the rupture and fusion of surface-adsorbed lipid vesicles and, ultimately, bilayer formation. Finally, the chamber was rinsed with D_2O to remove the liposomes remaining intact on the solid surface and in the bulk phase.

Three aqueous phases differing by their D_2O/H_2O ratio were used to vary the neutron contrast: pure D_2O, pure H_2O and 38% D_2O / 62% H_2O (V/V) corresponding to SiMW (silicon-matched

water), with a scattering length density (*SLD*) of 2.07×10^{-6} Å^{-2} matching the silicon substrate, combined to different bilayers compositions (d_{62}-DPPC, d_{62}-DPPC/TC or d_{62}-DPPC/TO) (Table 1). Prior to any measurement, the bare silicon substrates were characterised in D_2O and H_2O. Details on the analysis of the reflectivity data are given in Supporting Information.

Table 1: Calculated neutron *SLD* of each component (see also Supporting Information)

Component		Neutron SLD ($\times10^6$) (Å^{-2})
Solid substrate	Silicon (Si)	2.07
	Silicon oxide (SiO_x)	3.41
d_{62}-DPPC	d_{62}-tails	6.71
	h_{18}-head group	1.88[a]
DPPC	h_{80}-DPPC	0.25
Aqueous phase	D_2O	6.33
	SiMW	2.07
	H_2O	-0.56
BS	NaTC	0.95[b]
	NaTDC	0.90[b]
FA	Caprylic acid (C8:0)	0.19[c]
	Oleic acid (C18:1)	0.08[c]
MAG	Monocaprylin (C8:0)	0.35[c]
	Monoolein (C18:1)	0.20[c]
TAG	Tricaprylin (C8:0)	0.33[c]
	Triolein (C18:1)	0.15[c]

[a] The *SLD* value reported for the head group does not include any contribution from water hydration.

[b] The *SLD* of each BS was calculated using the following molecular volume (v_m) values: $v_{m\ NaTC}$ = 0.680 nm^3 [66], $v_{m\ NaTDC}$ = 0.658 nm^3 [33].

[c] The *SLD* of each FA, MAG and TAG was calculated using their mass density value: while the density of both FA and TAG was known (0.91 for C8:0 FA, 0.89 for C18:1 FA, 0.96 for C8:0 TAG and 0.91 for C18:1 TAG), the density of both MAG was assumed to be of similar value to that of FA and was fixed at 0.90 for the calculation of the *SLD*.

3. Small-angle X-ray and neutron scattering

Small-angle X-ray scattering (SAXS). SAXS measurements were performed on the high brilliance ID02 beamline, at the European Synchrotron Radiation Facility (ESRF, Grenoble, France) [67], using a 2-mm-inner diameter flow-through quartz capillary, thermostated by a Peltier module. Details of the instrument configuration are provided in Supporting Information.

Small-angle neutron scattering (SANS). SANS measurements were performed on the SANS2D time-of-flight instrument, at ISIS pulsed neutron source (STFC Rutherford Appleton Laboratory, Didcot, UK) [68] (for BS micelles and mixed micelles), and on the D33

spectrometer, at the Institut Laue-Langevin (ILL, Grenoble, France) [69] (for BS micelles and TAG-incorporating liposomes), using 1 mm path-length quartz cells (Hellma Analytics, Müllheim, Germany) thermostated with a circulating water bath. Details of the instrument configuration are provided in Supporting Information.

BS micelles. SAXS and SANS measurements were carried out on a range of BS aqueous solutions (2 - 200 mM) at 25°C, using ID02 and SANS2D, and at 37°C, using D33. The solutions of BS were prepared with and without salt (0.15 M NaCl), in either H_2O (SAXS) or D_2O (SANS) (Table 1; calculated electron *SLD* of H_2O: 9.47×10^{-6} Å^{-2}, NaTC: 12.05×10^{-6} Å^{-2}, NaTDC: 12.16×10^{-6} Å^{-2} (for further detail on the *SLD* calculation method, see Supporting Information)).

Mixed micelles. BS/FA and BS/MAG mixed micelles were prepared by vortex-mixing, followed by sonication with a probe sonicator for 30 s. Based on solubility tests (data not shown), FA (caprylic acid (C8:0) and oleic acid (C18:1)) and MAG (monocaprylin (C8:0) and monoolein (C18:1)) were employed at concentrations both close to and far from their solubility limit in BS micelles, which was higher for NaTDC (from 0.10 to 1.50% w/w) (Table S1). Each mixed micelle (BS/FA and BS/MAG) comprised 100 mM BS (well above BS CMC), to maximise the scattering. All micelles were prepared with and without salt (0.15 M NaCl) in D_2O and measured at 25°C by SANS (SANS2D).

Solubilisation of lipid vesicles into mixed micelles. The liposomes described in the previous section (DPPC, DPPC/TC and DPPC/TO), prepared with hydrogenated lipids (DPPC), were mixed with varying amounts of BS aqueous solutions, with at least 12 hours of equilibration before measurements. All samples were made in D_2O and were measured by SANS, at 25 and 37°C (D33).

Details on the data modelling are provided in Supporting Information.

4. Molecular dynamics simulations

All-atom molecular dynamics (MD) simulations were carried out to investigate the molecular-scale mechanisms governing the self-assembly of NaTC and NaTDC in a 0.15 M NaCl aqueous solution. Three different concentrations (10, 20 and 50 mM) were employed for each BS. Table 2 summarises the number of BS, water, sodium cations (Na^+) and chlorine anions (Cl^-) included

in each of the six simulated systems. The number of BS was chosen so that the number of BS molecules in the simulation is at least twice the average aggregation number (N_{agg}) determined from the experimental investigations.

Table 2: Number of BS, water, Na^+ and Cl^- in each simulated system.

BS type	[BS] (mM)	# BS	# Water	# Na^+	# Cl^-
NaTC	10	12	62709	190	178
	20	25	64461	208	183
	50	25	25009	96	71
NaTDC	10	12	62717	190	178
	20	25	64811	208	183
	50	25	25433	96	71

Each of these systems was initially built with the BS molecules and the salt ions randomly distributed in the simulation box using the CHARMM-GUI multicomponent assembler. After the initial systems were assembled, the same simulation protocol was followed for each system. First, a steepest descent energy minimisation was performed on each of the systems using a maximum of 5000 minimisation steps and an energy tolerance of 1000 kJ/mol. Then the minimised configurations were equilibrated at 303.15 K using the constant number, volume and temperature (NPT) ensemble, in which the Nosé-Hoover thermostat [70,71] was applied, for 25 ps. Finally, a production simulation was carried out for 150 ns at 300 K using the NPT ensemble with the Nosé-Hoover thermostat at 303.15 K and the Parrinello-Rahman barostat [72] at 1 bar.

All the simulations used the GROMACS simulation 2018 package [73,74]. The inter- and intra-molecular interactions of the BS, Na^+ and Cl^- were described with the CHARMM36 general force field [75]. The CHARMM-modified TIP3P water model [76], which is commonly used with the CHARMM force field [77], was used to model water molecules. The Lennard-Jones interactions were cut off at 10 Å, whilst the electrostatic interactions were cut off at 12 Å. The Particle-Mesh-Ewald (PME) method was used to compute long-range electrostatic interactions. Hydrogen-containing bonds were constrained using the LINCS algorithm [78], so that a 2 fs could be used in all simulations while ensuring stable integration of Newton's equations of motion with the velocity Verlet algorithm.

Analysis was performed using Python codes developed in-house, which make wide use of the MDAnalysis package [79,80]. BS clusters are identified by an algorithm that makes use of the

NetworkX package [81]. An undirected, unweighted graph *G(V, E)*, was defined, where nodes (*V*) represent individual BS molecules and edges (*E*) are assigned by a distance cutoff (C17 atoms within 9 Å of each other). The connected subgraphs of *G*, which represent clusters present at a given time, were subsequently identified. Contact maps were calculated by finding the number of interactions between different specified atoms within a distance cutoff (atoms within 9 Å of each other, the same distance as used in the clustering algorithm).

In order to determine the size of the BS clusters in our simulations, the radius of gyration (R_g) of each aggregate was calculated. The radius of gyration and eccentricity of an aggregate consisting of *N* atoms, each with mass m_i and position $\boldsymbol{r}_i$, are defined as:

$$R_g^2 = \frac{1}{M}\sum_{i=1}^{N} m_i|\boldsymbol{r}_i - \boldsymbol{r}_{COM}|^2 \quad (2) \qquad \text{Eccentricity} = 1 - \frac{I_{min}}{I_{av}} \quad (3)$$

where *M* is the sum of all atomic masses in the aggregate, and I_{min} and I_{av} the minimum and average of the cluster's moments of inertia. While the values calculated cannot directly be compared to the ones obtained from SANS data, where the eccentricity is defined as Eccentricity = $\sqrt{1 - \frac{R_{Pol}^2}{R_{Eq}^2}}$ (see Supporting Information, equation S10), the overall trends as a function of molecular species and concentration provide a means of comparison.

Results

1. Aggregation of BS in solution

Critical micellar concentration (CMC) of BS. The micellisation of NaTC and NaTDC in water was studied by fluorescence spectroscopy, using pyrene as a probe at two different temperatures (Figure 2, Table 3).

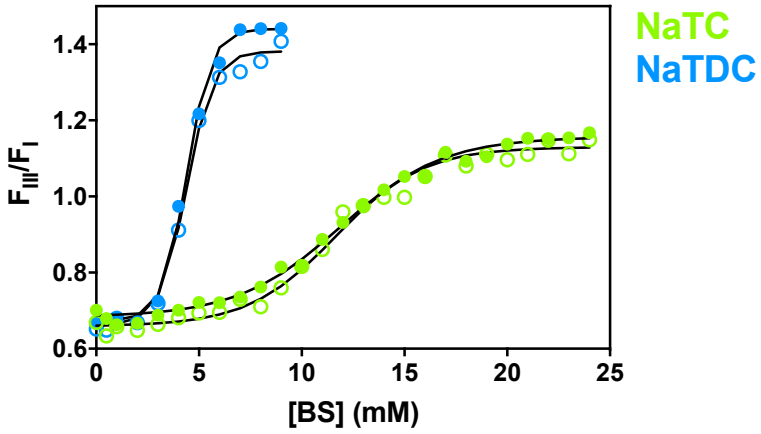

Figure 2: Evolution of pyrene emission fluorescence (F_{III}/F_I) in water as a function of the concentration in BS (NaTC, NaTDC), at two different temperatures: (○) 23°C, (●) 37°C. Solid lines are fits of the data to Equation (1).

	CMC (mM)		ΔF_{max}	
	23°C	**37°C**	**23°C**	**37°C**
NaTC	5 ± 2	5 ± 2	0.47	0.45
NaTDC	2 ± 0.5	2 ± 0.5	0.79	0.75

Table 3: *CMC* and ΔF_{max} values for each BS studied, at 23°C and 37°C.

For each BS, three regions can be distinguished: at low concentrations, BS are in the form of free unimers and pyrene emission is low as it is in a polar environment; as BS concentration increases, BS molecules start aggregating and incorporating some of the pyrene into a less polar environment (the micelles interior); at high concentrations, a plateau, characteristic of all of the pyrene being fully inside micelles, is reached. The two BS, however, present very distinct profiles (Figure 2): a smooth, gradual rise in F_{III}/F_I for NaTC, and a sharp increase for NaTDC occurring at low BS concentrations, as reported elsewhere [82–84]. These contrasting profiles are associated to different values of the *CMC* and ΔF_{max}, which are insensitive to temperature (in agreement with the literature [85]): NaTC has a much higher *CMC* than

NaTDC, but a much lower ΔF_{max} (Table 3, Equation (1)). The *CMC* values are consistent with literature data obtained using the same technique (NaTC: CMC = 3 – 5 mM; NaTDC: CMC = 2.9 mM) [84]. The higher value of ΔF_{max} obtained with NaTDC shows that pyrene probes a more hydrophobic environment in NaTDC micelles, compared to NaTC, in line with the lower polarity of NaTDC, which bears one less hydroxyl group.

Morphology of BS micelles. SANS and SAXS were used to examine the structure of NaTC and NaTDC micelles as a function of concentration, in the absence and presence of salt (0.15 M NaCl). Various models were assessed (sphere, cylinder, prolate ellipsoid and oblate ellipsoid), and the model that provided the best fit was the ellipsoid model. However, neither SANS nor SAXS could differentiate between oblate and prolate structures; data were fitted here considering plain oblate ellipsoids (Figures 3, 4, 5 and S5, Table S3).

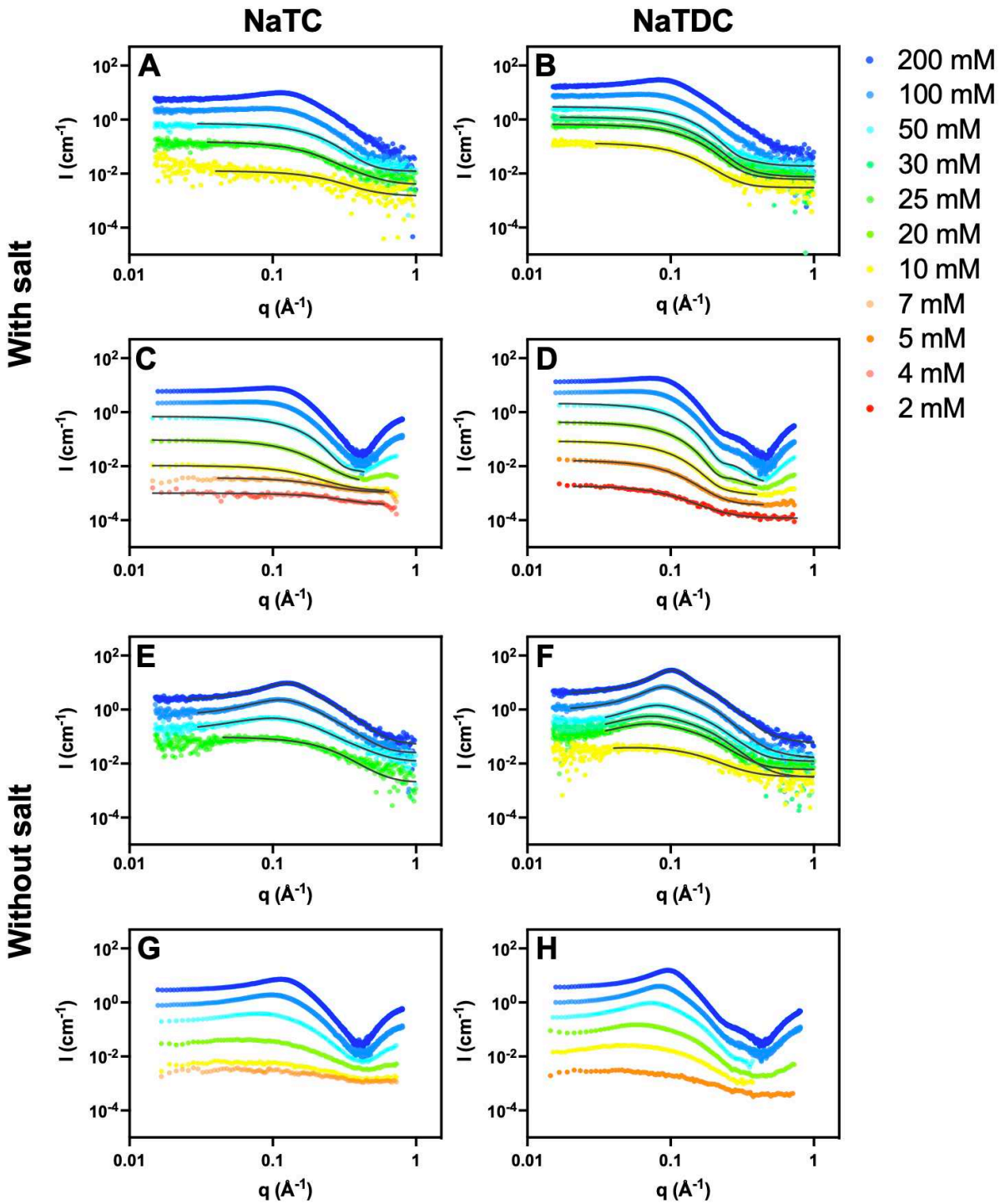

Figure 3: Scattered intensity (*I*) as a function of the scattering vector (*q*) for BS aqueous solutions of either NaTC (A, C, E, G) or NaTDC (B, D, F, H), prepared at different concentrations (from 2 to 200 mM), with (A, B, C, D) and without (E, F, G, H) 0.15 M NaCl, and measured at 25°C, by SANS (A, B, E, F) and SAXS (C, D, G, H). Solid lines correspond to fits to the data as described in the text (Equation (S6)). For readability purposes, curves are staggered vertically.

In the absence of salt, the two BS exhibit a peak characteristic of electrostatic interactions (Figures 3, E, F, G, H), which was described by a Hayter-Penfold potential in the SANS data (SAXS data with strong interactions present were not fitted). In the presence of NaCl, this peak disappears due to the screening of charges, except at the highest concentrations of BS, 100

and 200 mM (Figures 3, A, B, C, D); the structure factor was therefore neglected in the analysis of the SANS and SAXS data obtained with BS concentrations ranging between 2 and 50 mM, which are the data we focus on in the main text.

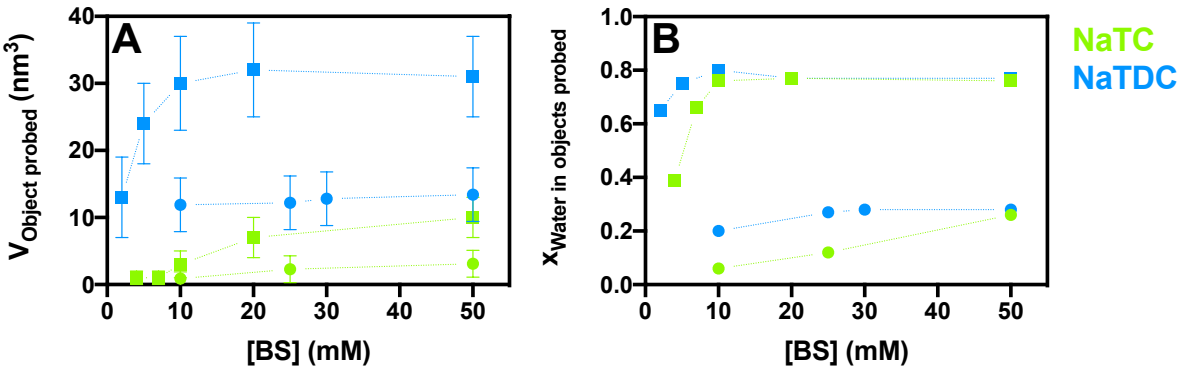

Figure 4: Evolution of (A) the volume of the object probed ($V_{Object\ probed}$), namely, the whole micelle with SAXS and the micellar core with SANS, and (B) the fraction of water in the object probed ($x_{Water\ in\ objects\ probed}$), as a function of BS concentration, with 0.15 M NaCl: (●) SANS, (■) SAXS. Errors on $x_{Water\ in\ objects\ probed}$ are smaller than the symbols.

In the presence of salt, larger aggregates were found by fitting the SAXS data, compared with SANS (e.g., with 50 mM NaTC, the volume ($V_{Object\ probed}$) obtained from SAXS is 10 ± 3 nm^3 compared to 3 ± 2 nm^3 with SANS; with NaTDC, it is 31 ± 6 nm^3 with SAXS *vs*. 13 ± 4 nm^3 with SANS), suggesting that the micelles have a hydrated region (or 'shell'), which is not detected by neutrons (Figure 4A, Table S3). SAXS measurements performed in D_2O demonstrated that the solvent (D_2O *vs.* H_2O) had no impact on the micellar structure (data not shown). However, SAXS data could not be fitted to a core/shell model either, suggesting that this corona region is not well defined. The extent of micellar hydration ($x_{Water\ in\ objects\ probed}$) returned by the fits was higher in the SAXS data, in agreement with SAXS probing this region better (Figure 4B, Table S3). Based on this assumption, the aggregation number (N_{agg}) and volume ($V_{Micelle}$) of each BS micelle, as well as the amount of water in micelles ($x_{Water\ in\ micelles}$) and the micellar volume fraction ($\Phi_{Micelles}$), were determined from SAXS data, while the volume of the core ($V_{Micelle\ core}$) and the extent of hydration in the core ($x_{Water\ in\ the\ core}$) were obtained from SANS.

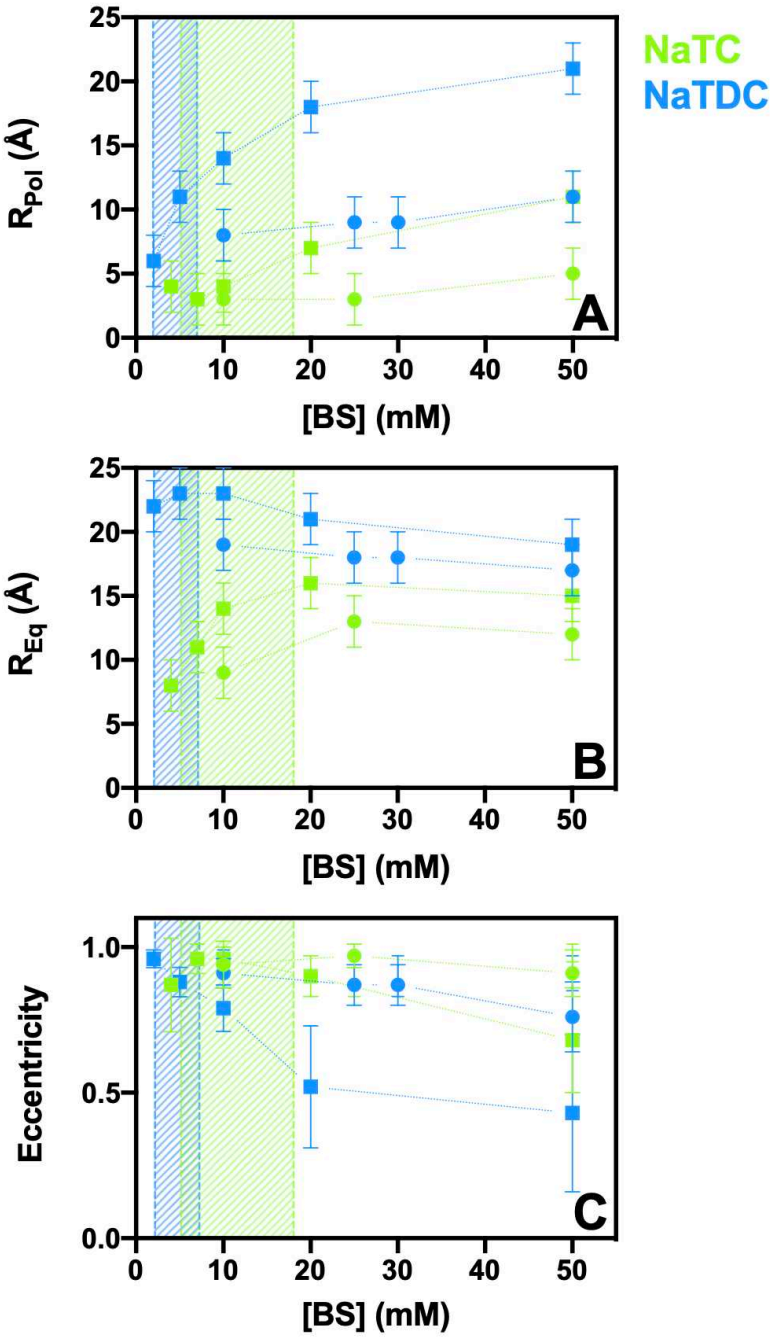

Figure 5: Evolution of (A) the polar radius (R_{Pol}), (B) the equatorial radius (R_{Eq}) and (C) the eccentricity of the object probed (namely, the whole micelle with SAXS and the micellar core with SANS), as a function of BS concentration, with 0.15 M NaCl: (●) SANS, (■) SAXS. Hashed areas indicate the BS concentration range below which BS (NaTC, NaTDC) are present in the form of unimers only (N_{agg} = 1) and over which micellisation occurs, based on pyrene fluorescence spectroscopy data (Figure 2).

Both in the absence and presence of salt, much smaller objects (both below and above the CMC) ($V_{Micelle\ core}$, $V_{Micelle}$, N_{agg}) are obtained with NaTC, compared to NaTDC (e.g., with 50 mM BS and 0.15 M NaCl, N_{agg} = 4 ± 1 for NaTC *vs*. N_{agg} = 11 ± 2 for NaTDC) (Figure 4A, Table S3). This is consistent with values from the literature (NaTC: N_{agg} = 3 – 7, NaTDC: N_{agg} = 12 – 19)

[16,19]. Such small micellar sizes are consistent with the peculiar structure of BS, where efficient packing is hindered by the planar shape of the hydrophobic region.

Additionally, for both BS, under both salt conditions, micellar size increases with concentration ($V_{Micelle\ core}$, $V_{Micelle}$, N_{agg}) (e.g., from 10 to 50 mM with NaCl, N_{agg} increases from 1 ± 1 to 4 ± 1 for NaTC, and 9 ± 2 to 11 ± 2 for NaTDC) (Figure 4A, Table S3), suggesting a gradual process of self-assembly. This increase in micellar size is particularly notable in the lower concentration range, up to ca. 20 mM for NaTC and ca. 10 mM for NaTDC, in agreement with the fluorescence data (Figure 2), which showed that micellisation takes place over a wide range of concentrations, particularly for NaTC. Above these concentrations, the micellar size (N_{agg}) stabilises to ca. 4 ± 1 and 11 ± 2 for, respectively, NaTC and NaTDC. The ellipsoids formed by the two BS grow mostly in the direction of their polar radius (R_{Pol}), from ca. 4 ± 2 Å to 11 ± 2 Å with 10 to 50 mM NaTC, and from ca. 6 ± 2 Å to 21 ± 2 Å with 2 to 50 mM NaTDC (Figure 5A, Table S3), with their equatorial radius (R_{Eq}) remaining stable around 15 ± 2 Å for NaTC and 22 ± 2 Å for NaTDC (Figure 5B, Table S3) (with salt, from SAXS data). At high concentrations, NaTDC aggregates adopt a more isotropic shape (e.g., at 50 mM BS, R_{Pol} = 21 ± 2 Å and R_{Eq} = 19 ± 2 Å, from SAXS data) (Figures 5, A, B, Table S3). The radii values obtained in this study are in the range of BS dimensions, the molecule being approximately 20 Å long and 7 Å wide [2]. Overall, upon increasing BS concentration to 50 mM, the micelle eccentricity decreases from ca. 1.00 to 0.68 ± 0.18 and 0.43 ± 0.27 for NaTC and NaTDC, respectively, indicating a transition from ellipsoidal to more spherical shapes, more marked with NaTDC (Figure 5C). Previous SAXS studies on NaTDC in tris buffer used a similar model (oblate biaxial ellipsoid), obtaining comparable sizes [26].

As expected, the presence of salt results in larger micellar sizes ($V_{Micelle\ core}$) for NaTDC (e.g., $V_{Micelle\ core}$ increases from 8 ± 3 to 13 ± 4 nm^3, at 50 mM, upon addition of 0.15 M NaCl), whereas the aggregates formed by NaTC display the same, significantly smaller volume both in the absence and presence of salt (e.g., $V_{Micelle\ core}$ = 3 ± 2 nm^3, at 50 mM) (Figure 4A, Table S3).

Measurements were also performed at 37°C, in the absence of salt, and showed that temperature has no impact on BS micellar dimensions and structure, regardless of BS type and concentration (Figure S5).

Molecular organisation of BS in micelles. MD simulations were performed in order to obtain further insight into the molecular arrangement of each BS in their micellar aggregates, at 10, 20 and 50 mM, in the presence of salt (0.15 M NaCl) (Figures 6, 7, 8, S6 and S7, Tables S4 and S5).

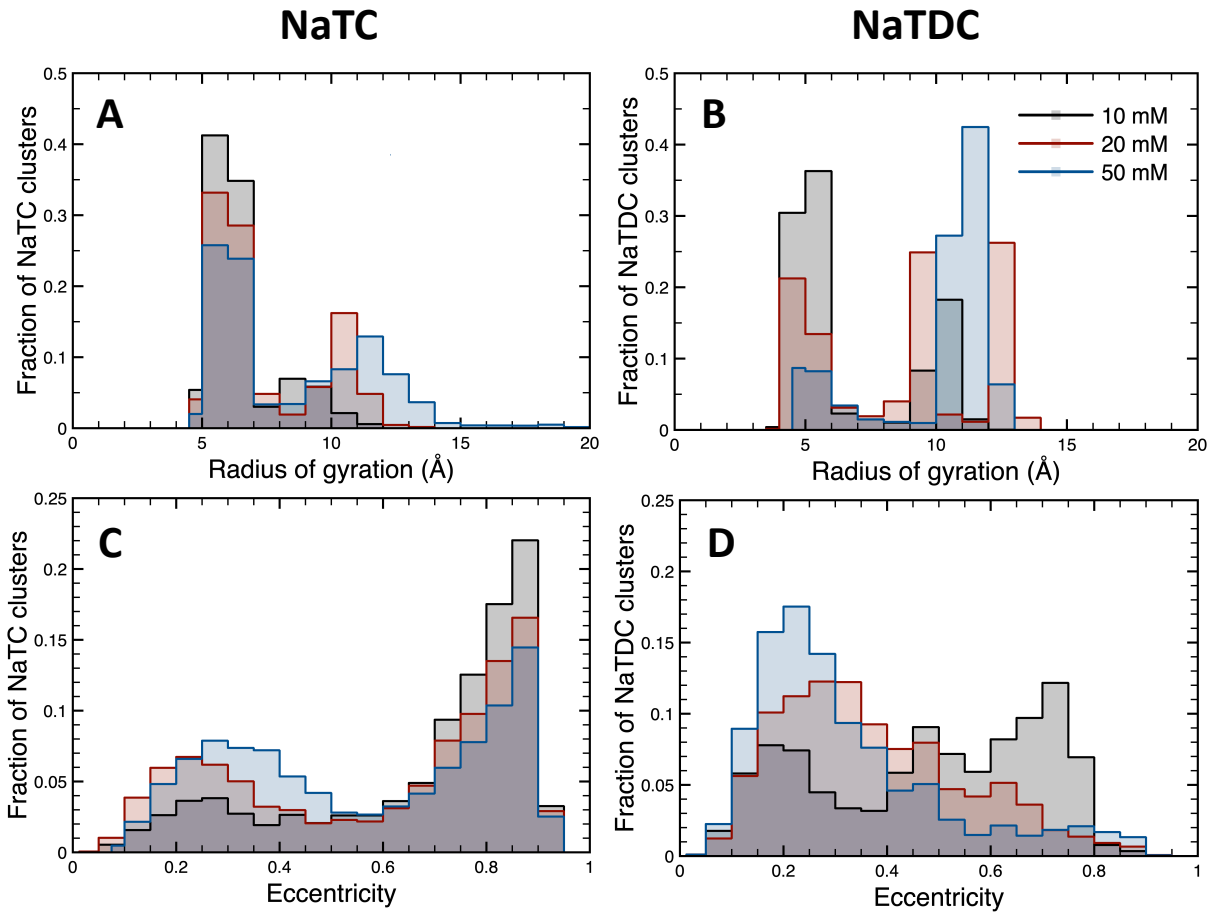

Figure 6: Probability distribution of (A, B) the radius of gyration and (C, D) the eccentricity of the aggregates, including unimers, obtained for BS aqueous solutions of either NaTC (A, C) or NaTDC (B, D), at different concentrations (10, 20 and 50 mM), in the presence of 0.15 M NaCl.

For both BS, a decrease in the number of isolated unimers in solution and an increase in the average cluster size are observed as BS concentration increases, thereby showing that BS molecules self-aggregate into increasingly large micelles, more notably so with NaTDC (Figure S6, Table S4), in agreement with the scattering data (Figure 4A, Table S3). This result is consistent with the evolution of the radius of gyration of the micelles (of size greater than one BS molecule), which shifts to higher values with increasing amounts of BS, varying from 8.6 ± 1.2 Å at 10 mM, to 9.6 ± 1.6 Å at 20 mM and to 10.9 ± 2.2 Å at 50 mM, for NaTC (Figure 6A, Table S4), and from 9.8 ± 1.1 Å at 10 mM, to 10.7 ± 1.8 Å at 20 mM and to 11.1 ± 1.0 Å at 50

mM, for NaTDC (Figure 6B, Table S4). Additionally, in contrast to NaTC, where a significant number of free unimers was present at the lowest concentrations, very few NaTDC molecules were found as isolated unimers in solution at any concentration, which is in line with the CMC measurements (Table 3). Results also show that the eccentricity of BS aggregates (of size greater than one molecule) does not change much upon increasing BS concentration, remaining approximately equal to 0.30 and 0.25 at all concentrations for NaTC and NaTDC, respectively (Table S4). When also taking the free unimers into account, a decrease in eccentricity is observed for both BS upon increasing BS concentration, from 0.68 ± 0.23 at 10 mM, to 0.59 ± 0.27 at 20 mM and to 0.55 ± 0.25 at 50 mM, for NaTC (Figure 6C, Table S4), and from 0.48 ± 0.22 at 10 mM, to 0.37 ± 0.18 at 20 mM and to 0.32 ± 0.18 at 50 mM, for NaTDC (Figure 6D, Table S4), which is in very good agreement with the scattering studies (Figure 5C).

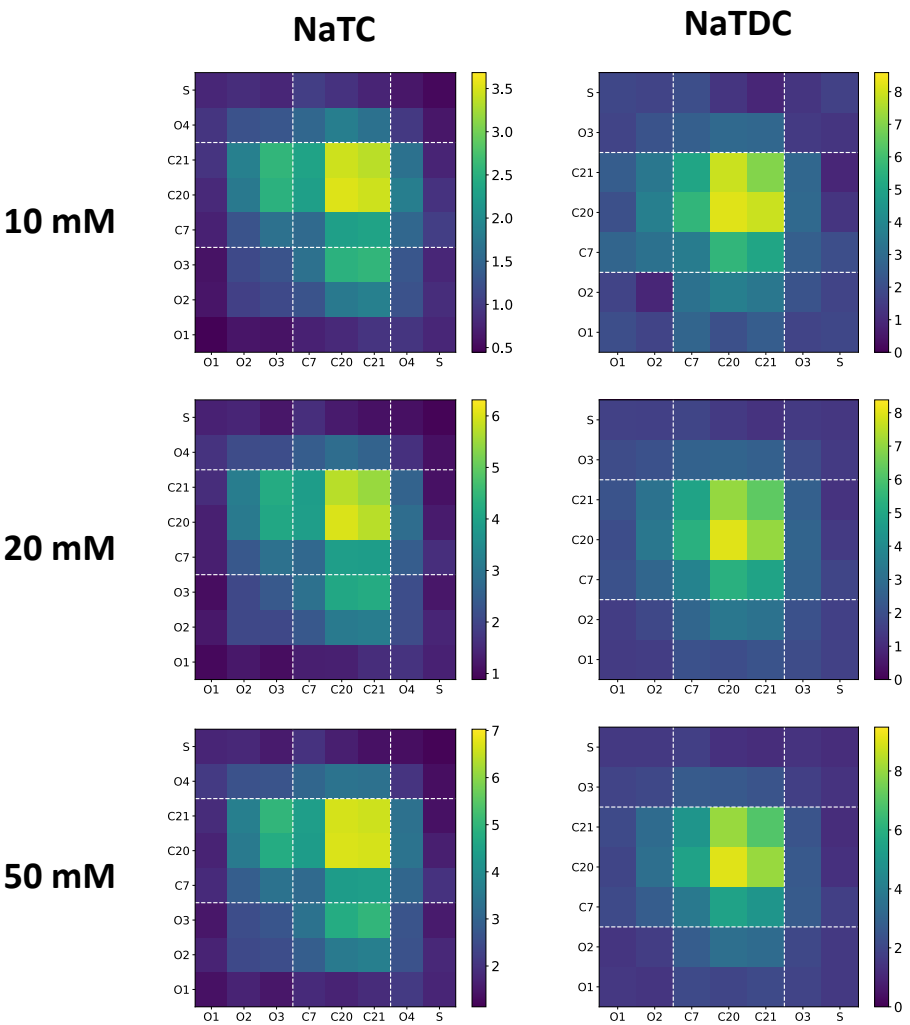

Figure 7: Contact maps showing the intermolecular interactions that drive the self-assembly process of BS molecules (NaTC, NaTDC), at different concentrations (10, 20 and 50 mM), in the presence of 0.15 M NaCl. The atom labels used on the two axes are defined in Figure S7.

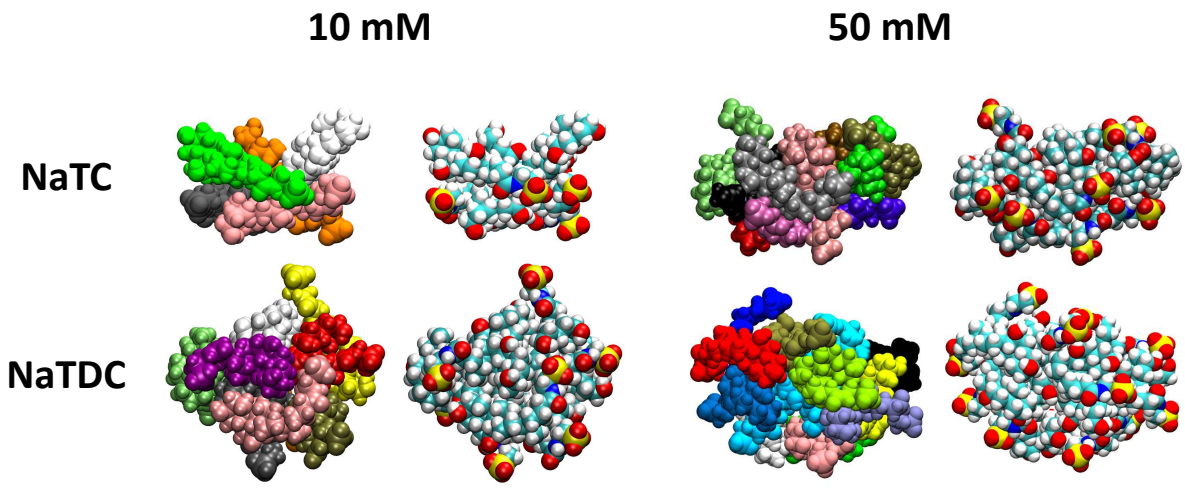

Figure 8: Snapshots from the MD simulations of BS micelles (NaTC, NaTDC) formed at different concentrations (10 and 50 mM), in the presence of salt (0.15 M NaCl). NaTC forms on average 1 aggregate of 5 molecules at 10 mM, 3 aggregates of 7 molecules at 20 mM, and 2 aggregates of 10 molecules at 50 mM, while NaTDC self-assembles into approximately 1 micelle of 8 molecules at 10 mM, 2 micelles of 11 molecules at 20 mM, and 2 micelles of 11 molecules at 50 mM. Colours are used to highlight either the different BS molecules or the different atoms. The micelles shown in this figure are not perfectly to scale.

Contrary to BS methyl groups (C_7, C_{20}, C_{21}), which show the highest intermolecular contact probabilities, the sterol hydroxyl groups (O_1, O_2 and O_3 for NaTC, O_1 and O_2 for NaTDC) and ionic chain amide oxygen and sulfur atoms (O_4 and S for NaTC, O_3 and S for NaTDC) do not significantly interact in the self-assembled BS micelles (Figure 7); these observations confirm that BS self-aggregation is primarily driven by hydrophobic interactions occurring between BS hydrophobic faces, the hydrophilic moieties contributing much less to BS bulk aggregation behaviour. Such bulk hydrophobic self-associations have also been observed with biomolecules [86]. Intermolecular contacts increase in magnitude with increasing BS concentration, reflecting the increase in aggregate size. Compared to NaTC, NaTDC molecules interact more strongly with each other, at all concentrations, thereby confirming the higher propensity of NaTDC – the more hydrophobic BS – for bulk aggregation. The arrangement of BS molecules in their micelles can be seen in the snapshots shown in Figure 8.

2. Aggregation of BS with FA and/or MAG in mixed micelles

Shape and size of BS mixed micelles. The scattering from BS micelles in the presence of FA or MAG, typical products obtained from the lipolysis of TAG, was fitted with the same ellipsoid model (Figures 9, S8 and S9, Table S6).

Similarly to BS micelles, the low scattering signals ($I(0) < 100\ cm^{-1}$) and the peaks of interaction, which disappear in the presence of salt (0.15 M NaCl), suggest that the mixed aggregates are relatively small and interact through electrostatic interactions, unless charges are screened by salt (Figures S8 and S9).

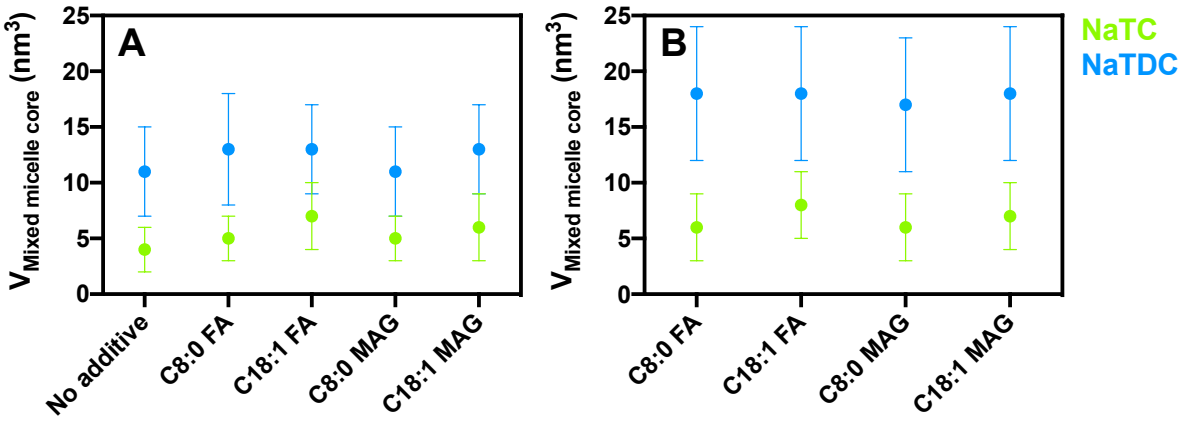

Figure 9: Evolution of the volume of the BS mixed micelles (100 mM) obtained from SANS data ($V_{Mixed\ micelle\ core}$), in the (A) absence and (B) presence of 0.15 M NaCl, with various additives at a low concentration (0.25% w/w). Results obtained with pristine BS (NaTC, NaTDC) micelles, in the absence of additives, with salt, are also indicated for comparison.

Under all conditions, BS/FA and BS/MAG mixed micelles are marginally larger than BS neat micelles (Figure 9A, Table S6), and NaTDC was found to form larger mixed aggregates, compared to NaTC, independently of the ionic strength, type and structure of FA or MAG, and concentration (up to 1.5% w/w) (Figure 9, Table S6), therefore suggesting that NaTDC solubilisation capacity is larger than NaTC (although this was not studied systematically). Values of the volumes obtained from SANS ($V_{Mixed\ micelle\ core}$) range between 3 – 19 nm^3 and 7 – 33 nm^3 for, respectively, NaTC and NaTDC mixed aggregates, whereas $V_{Micelle\ core} = 4 \pm 2\ nm^3$ and $11 \pm 4\ nm^3$ for, respectively, NaTC and NaTDC pure micelles, without salt.

Comparing the results obtained with the same concentration of additive (0.25% w/w), both the type of additive (FA *vs*. MAG) and the chain length and saturation (C8:0 *vs*. C18:1) affect micellar size (Figure 9, Table S6). In the presence of oleic acid and monoolein (C18:1), BS mixed aggregates are marginally larger than with, respectively, caprylic acid and monocaprylin (C8:0) (e.g., $V_{Mixed\ micelle\ core} = 13 \pm 4\ nm^3$ with C18:1 MAG *vs*. $V_{Mixed\ micelle\ core} = 11 \pm 4\ nm^3$ with C8:0 MAG, for NaTDC, without salt); however, the difference is small and would require a larger systematic study to be confirmed - as well as is testing the limits of SANS detection given the small radii sizes (Table S6). A larger micellar size with longer lipid chain length has been

observed previously with the addition of both FA and MAG to BS/phospholipids mixed micelles [87].

The addition of salt causes an increase in micellar size under all conditions, and to a larger extent for NaTDC, as compared to NaTC, thereby showing the incorporation of a larger amount of additives and/or BS molecules into the aggregates in the presence of salt (Figure 9, Table S6). For instance, $V_{Mixed\ micelle\ core}$ increases from 14 ± 5 to 41 ±11 nm^3 and from 26 ± 7 to 41 ± 11 nm^3 for NaTC and NaTDC, respectively, in the presence of 1.50% w/w C8:0 FA.

3. Solubilisation of TAG-incorporating lipid vesicles into mixed micelles

Prior to evaluating the effect of the two BS on TAG-containing liposomes, the bilayer structure of each lipid vesicle was analysed by NR.

DPPC/TAG SLB structure. Using NR, the internal morphology of each TAG-incorporating lipid bilayer (d_{62}-DPPC, d_{62}-DPPC/TC and d_{62}-DPPC/TO) was characterised at the sub-nanometre length scale with contrast variation (Figures 10 and S10, Table S7).

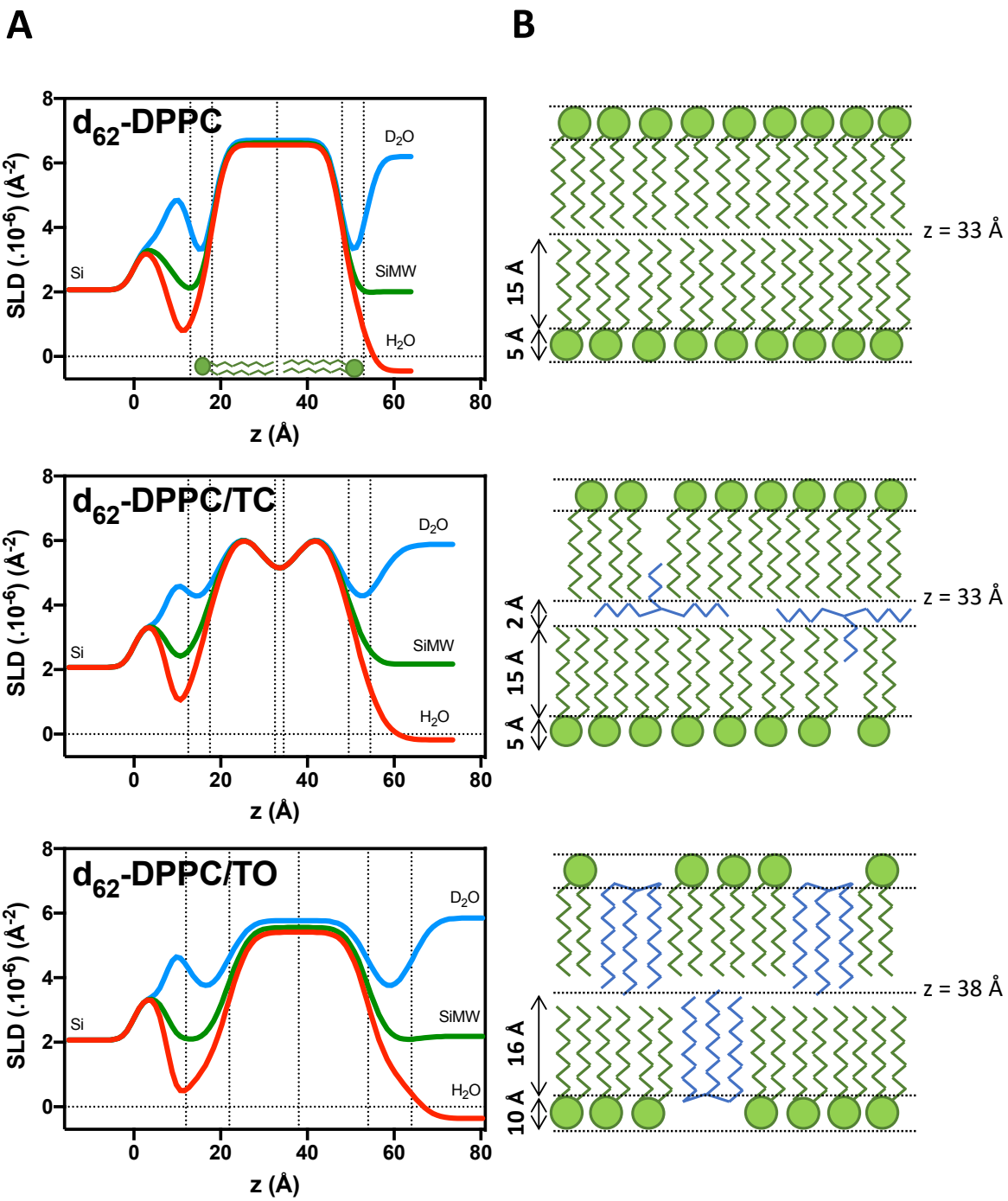

Figure 10: (A) Scattering length density (*SLD*) profile of each SLB: d_{62}-DPPC, d_{62}-DPPC/TC, d_{62}-DPPC/TO, in three different aqueous phases: (●) D_2O, (●) SiMW, (●) H_2O, along the direction perpendicular to the sample surface (*z*), obtained from the analysis of the reflectivity curves measured at 50 ± 2°C. Fits of the experimental data corresponding to these profiles are shown in Figure S10. (B) Schematic representation of each SLB, showing the location and organisation of each TAG (blue molecules) in the DPPC (green molecules) bilayer. Tricaprylin lies between the two tail regions of the DPPC bilayer, with two branches perpendicular to them and one parallel, whereas triolein is incorporated into the tails regions. Tricaprylin molecules may also display a Ⱶ-shape conformation; nonetheless, these measurements do not allow the determination of the ratio between the two configurations. The sketches are not completely to scale and represent an ideal system, the real samples being naturally characterised by a larger degree of disorder.

As expected, d_{62}-DPPC was found to form a symmetric SLB, with one homogeneous tail region and two hydrophilic head group layers. The data for the d_{62}-DPPC/TC SLB were fitted by a model in which the *SLD* profile shows a smooth dip in correspondence with the midplane of the bilayer, which is interpreted as an accumulation of tricaprylin molecules exhibiting a T shape, with two branches located between the two lipid tail regions (perpendicular to them) and one inserted within the tails (parallel to them) (Figure 10, Table S7). This arrangement resembles that of cholesterol in polyunsaturated lipid bilayers [88]. Because triolein hydrophilic moiety is quite insignificant compared to its hydrophobic region, triolein was hypothesised to insert into both lipid tails layers only (not into their head groups), as suggested elsewhere [60,89]. Compared to the d_{62}-DPPC/TC SLB, the drop in the tails *SLD* was uniform, therefore indicating that no additional central layer was formed (unlike tricaprylin), but that hydrogenated triolein molecules inserted in parallel to the d_{62}-DPPC tails. The considerable rise in both the amount of water in d_{62}-DPPC head groups (f_{water}) and in their layers thickness (t) may be explained by the presence of triolein in the tails, resulting in more solvated head group regions because of the more disordered packing (both vertically and laterally) induced by the inclusion of triolein. The lateral organisation of triolein molecules within the bilayer cannot be resolved in specular reflectometry measurements; therefore, the parameters cannot indicate whether triolein is evenly distributed or organised into domains. Further detail on each fitting procedure is given in Supporting Information.

DPPC/TAG liposomes structure. Going back to solution behaviour, the morphology of DPPC liposomes was first analysed by SANS (Supporting Information, Figure S11). Data fitting using the vesicular model described in [90] demonstrates the presence of both uni- and multi-lamellar vesicles with average radii of 11 and 42 nm, respectively. Further detail on the fitting procedure is given in Supporting Information. The structure of the TAG-incorporating liposomes (DPPC/TC and DPPC/TO) could not be described by the same model, or by various combinations of uni- and multi-lamellar vesicles; hence, data were described qualitatively.

Impact of BS on liposomes structure. The effect of BS on the structure of TAG-incorporating liposomes (DPPC, DPPC/TC and DPPC/TO) was investigated by SANS, at 25 and 37°C (Figures 11, S12 and S13, Table S8). First, the existence of three different phases was established (visually) based on BS concentration and type: (i) from 5 to 30 mM for NaTC, and from 5 to 10 mM for NaTDC, turbidity decreases, compared to the pure lipid vesicles; (ii) at 50 mM for

NaTC, and from 20 to 30 mM for NaTDC, mixtures undergo phase separation over time, giving rise to a transparent phase and a very opaque one (samples were measured before phase separation was completed); (iii) at 100 mM for NaTC, and 50 mM for NaTDC, solutions look completely transparent. Based on these results, three BS concentrations (10, 50 and 100 mM for NaTC, and 10, 30 and 50 mM for NaTDC), representative of each phase observed, were selected for this study.

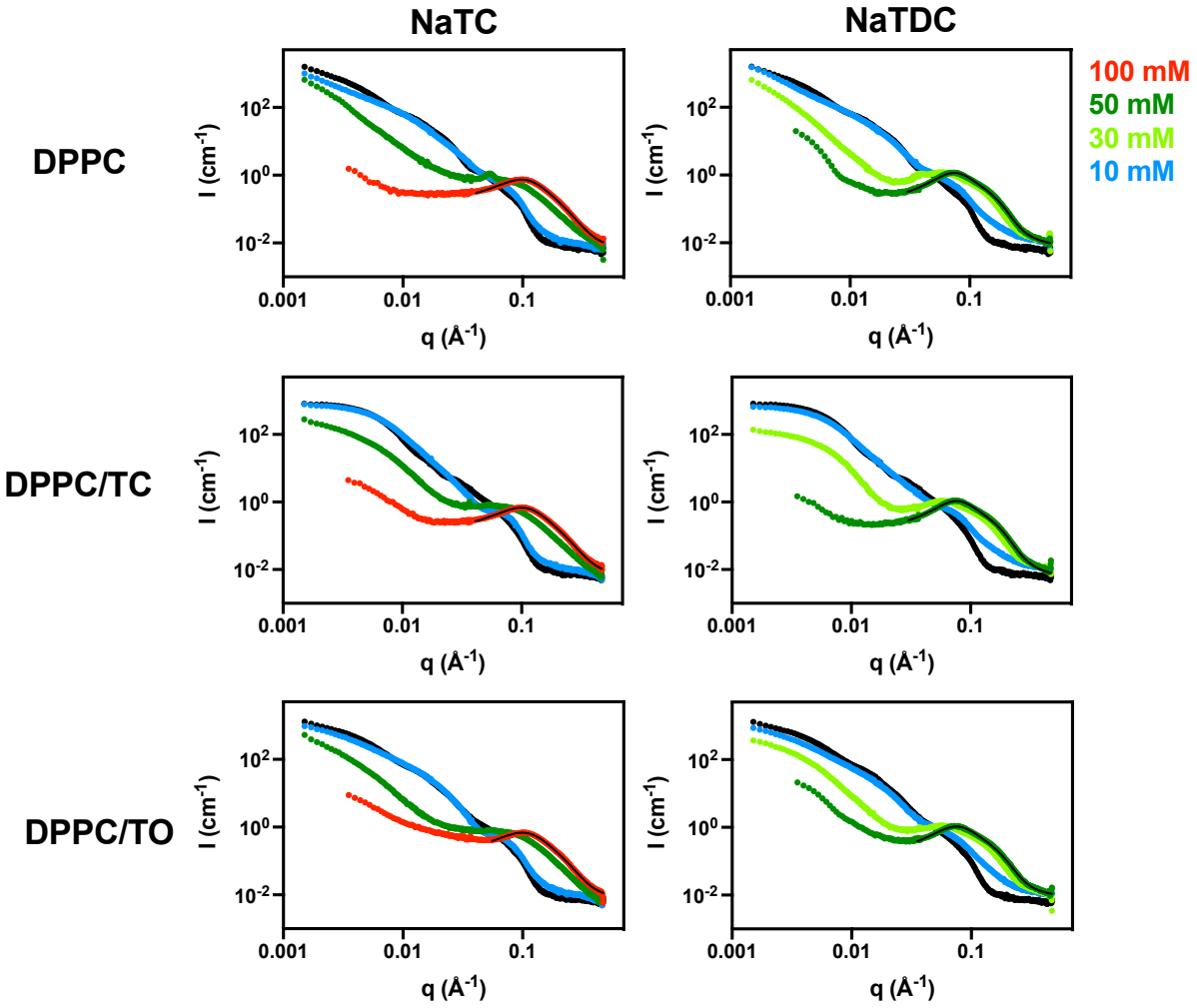

Figure 11: Scattered intensity (*I*) as a function of the scattering vector (*q*) for each TAG-incorporating lipid (DPPC, DPPC/TC, DPPC/TO) vesicle, mixed with different amounts (10, 30, 50 and 100 mM) of BS (NaTC, NaTDC), measured at 25°C, by SANS. The scattering curve of the pure liposomes (●) is also shown for comparison. The solid line is the trend line that best fits the data set (Equation (S3)).

SANS results confirm the presence of distinct structures in the three concentration ranges chosen (Figure 11): (i) at low concentrations (10 mM for both BS), each liposome undergoes very limited structural changes; (ii) in the intermediate concentration range (50 mM for NaTC, 30 mM for NaTDC), the intensity decreases, suggesting solubilisation of some of the vesicles

into BS micelles, while an interaction peak develops, suggesting intermicellar interactions; (iii) at high concentrations (100 mM for NaTC, 50 mM for NaTDC), the signal originates mostly from smaller interacting objects, such as micellar aggregates, while most of the liposomes have disintegrated.

The structures generated upon the addition of low and intermediate quantities of BS were not analysed due to the presence of multiple structures over a range of length scales, which would have required several assumptions to be made. The disruption of the liposome morphology is likely due to the adsorption and/or incorporation of BS molecules onto/into the vesicles bilayers, inducing a gradual vesicle-to-micelle transition, as suggested elsewhere with sodium cholate [42,44,91–93], sodium deoxycholate [42,44,91] and NaTC [56] with DPPC vesicles. Interestingly, the evolution of the scattering curves (Figure 11) is reminiscent of mixtures of the zwitterionic surfactant oleyl amidopropyl betaine with AOT (an anionic surfactant) and NaCl, recently reported [94]; upon reducing salt content, the curves show a similar structural evolution, which was analysed with a model comprising a mixture of vesicles with ellipsoidal/cylindrical micellar aggregates.

The scattering from the aggregates at high BS concentrations was fitted with the ellipsoid model described above (Figure S12, Table S8). The mixed aggregates are larger than BS micelles in both directions (R_{Pol} and R_{Eq}), and differences are more significant with NaTDC, as compared with NaTC (e.g., R_{Pol} = 8 ± 2 nm^3 for NaTC *vs*. R_{Pol} = 10 ± 2 nm^3 for NaTDC, and R_{Eq} = 16 ± 2 nm^3 for NaTC *vs*. R_{Eq} = 19 ± 2 nm^3 for NaTDC, in the presence of DPPC/TO). These results demonstrate that the addition of BS to liposomes leads to the gradual solubilisation of DPPC/TAG into BS mixed micelles, transitioning through various morphologies and their mixtures, and that the structures present depend on the type of BS; NaTDC solubilises liposomes at lower concentrations than NaTC and, as observed for the pristine micelles, its mixed aggregates are larger.

Interestingly, temperature has a significant impact on the ability of BS to solubilise lipids into mixed micelles (Figure S13). At physiological temperature (37°C), liposome solubilisation occurs at a lower BS concentration for both BS, resulting in a mixed micelles predominant phase from 50 mM for NaTC (against 100 mM, at 25°C) and 30 mM for NaTDC (against 50 mM, at 25°C).

The same phases are obtained in the same BS concentration ranges for all liposome compositions (DPPC, DPPC/TC, DPPC/TO), at both temperatures (25 and 37°C) (Figures 11 and S13, Table S8), despite the different location of the TAG within the liposomes (Figure 10).

Discussion

The objective of this work was to bring an understanding to the aggregation process of BS, focusing on the role of their molecular architecture, which is expected to control their behaviour at the lipid/water interface and, therefore, could explain their contrasting functionalities during fat digestion [14,16]. For this purpose, the structure of BS micelles, as well as of the mixed micelles they form in the presence of FA or MAG (the main products of lipolysis), was characterised, and the ability of BS to solubilise TAG-incorporating liposomes, mimicking ingested lipids, was evaluated. NaTC and NaTDC, two BS differing by the number of hydroxyl groups on their bile acid moiety (Figure 1), were selected based on previously reported distinct adsorption/desorption properties [14–16].

Bulk aggregation behaviour of BS, in the absence and presence of the products of lipolysis

The study of BS micellisation revealed two distinct self-assembly processes (Figure 2, Table 3): NaTC, unlike NaTDC and classic surfactants, micellises over a broad range of concentrations; overall, the CMC of NaTC (CMC = 5 ± 2 mM) is higher than NaTDC (CMC = 2 ± 0.5 mM), which correlates with the hydrophobicity of the two BS [95]. SANS (Figures 3, A, B, E, F) and SAXS (Figures 3, C, D, G, H) data were compatible with ellipsoid micelles, while SAXS data detected larger (Figure 4A) and much more hydrated objects (Figure 4B) than SANS, as neutrons were probably not sensitive to the more hydrated regions of the aggregates. However, a model with distinct core and shell could not be used, suggesting the absence of a clear core/shell segregation characteristic of conventional surfactants. Atomistic MD simulations confirmed that BS molecules self-assemble *via* their hydrophobic steroid skeleton, their ionic chain and hydroxyl groups being in contact with the bulk water (Figures 7 and 8). Independently of the ionic strength, NaTC aggregates are much smaller than NaTDC micelles (Figures 4A and 6, A, B); this size difference can be attributed to their relative hydrophobicity: NaTC has one more hydroxyl group and hydrophobic interactions are thus weaker. Both BS micelles exhibit a transition from an ellipsoidal to a more spherical shape upon increasing BS concentration, which is more marked for NaTDC (Figures 5C and 6, C, D). MD simulations reveal that this transition is mostly due to the presence of a large number of unimers, which cannot be decoupled from the micelles in the scattering data, and are in larger number for

NaTC (Figure 6), which is in agreement with the gradual micellisation process obtained from pyrene fluorescence (Figure 2).

During the lipolysis process, the products from lipid digestion (FA and MAG) accumulating at the lipid droplet interface are removed from the fat droplet surface by BS and solubilised into mixed micelles. The addition of FA (caprylic (C8:0) or oleic (C18:1) acid) or MAG (monocaprylin (C8:0) or monoolein (C18:1)) to BS solutions induced an increase in aggregates size, suggesting the incorporation of the additives into the BS micelles (Figure 9A), as also reported elsewhere in the presence of monoolein and oleic acid, with either a glycoconjugate (like sodium glycocholate or sodium glycochenodeoxycholate) [96] or L-alpha-phosphatidylcholine from egg yolk and NaTDC [97]. Compared to NaTC, NaTDC was found to solubilise higher amounts of FA (data not shown) and to form larger mixed micelles in the presence of additives (Figure 9), thus demonstrating NaTDC higher solubilising efficiency, forming larger aggregates as a result. In other studies, with other polar lipids, such as monoolein [98], phospholipids [42–44,53,91] and lecithin [47], the solubilising capacity of BS dihydroxy conjugates has also been demonstrated to be higher than that of trihydroxy conjugates.

Solubilising capacity of BS

Following our study on BS interaction with a phospholipid (1,2-dipalmitoyl-*sn*-glycero-3-phosphocholine, DPPC) monolayer at the air/water interface [14], used as a preliminary mimic of fat droplet interfaces, we have modelled ingested lipids using TAG-incorporating liposomes and investigated their fate in the presence of BS.

NR measurements show that the localisation of TAG molecules in DPPC bilayers depends on the TAG structure (i.e., chain length and saturation). More specifically, tricaprylin (or C8:0 TAG) inserts into the phospholipid vesicles by forming an additional layer between the two inner tails regions and incorporates part of its skeleton into the lipid hydrophobic layers, whereas triolein (or C18:1 TAG) is embedded in the lipid tails (Figure 10). While the bulk morphology of the TAG-incorporating lipid (DPPC/TC and DPPC/TO) vesicles could not be resolved, pure DPPC liposomes were shown to comprise a mixture of rather polydisperse uni- and multi-lamellar lipid vesicles, whose average radius is respectively equal to 11 and 42 nm (Figure S11).

SANS data analysis revealed that BS have a substantial impact on liposome structure, driving a gradual transition from liposomes to mixed micelles (Figure 11). Compared to NaTC, lower amounts of NaTDC are needed to induce this transition, leading to a mixed micelles-predominant phase (and near complete disruption of liposomes) at 30 mM, compared to 50 mM for NaTC, at 37°C (Figure S13); this correlates with NaTDC higher hydrophobicity [95] and is consistent with observations made in the presence of sodium cholate *vs*. sodium deoxycholate [42,44,91]. Therefore, this study provides evidence that NaTDC exhibits a better solubilising capacity than NaTC, which supports our working hypothesis that deoxycholate-based BS are more likely to be involved in the incorporation of lipolysis products into mixed aggregates, for absorption in the gut mucosa, compared to cholate derivatives, which, instead, may have a higher efficacy at facilitating enzyme adsorption onto the surface of fat droplets.

Conclusion

Our working hypothesis is that the contrasting roles played by BS during the process of fat digestion may be explained by architectural differences in their bile acid moiety. We therefore compared the aggregation properties of two BS, NaTC and NaTDC, (known to present contrasting interfacial properties), and also characterised the mixed micelles they formed with liposomes and typical products of lipolysis (FA and MAG).

Despite extensive investigations, BS micellisation process and micellar structures are, to date, still a topic of controversy. The unique combination of scattering techniques and atomistic simulations employed in this work brings a fundamental, molecular-level picture of structures relevant to the process of lipid digestion, whose knowledge is crucial to unlock the processes involved in lipid digestion and, ultimately, develop therapeutic strategies to control and optimise the absorption of lipids contained in food formulations. Specifically, our results show that the two structurally distinct BS display a different micellisation behaviour, leading to different sizes and shapes. NaTDC exhibits a lower, sharper CMC, and forms more spherical, larger micelles than NaTC, whose micellisation takes place over a broad range of concentrations. BS planar hydrophobic faces, which drive micellisation, imply that the morphologies depart from a conventional core/shell structure. NaTDC has a higher capacity to solubilise FA and MAG (used as models of lipolysis products) and forms larger aggregates. TAG-incorporating liposomes – employed here to mimic a fat interface coming into contact with BS molecules in the gut – are gradually solubilised by both BS into mixed micelles, but lower concentrations of NaTDC are required to achieve the same outcome, compared to NaTC.

In addition to providing a detailed characterisation of BS self-assembly behaviour and the structures formed with lipolysis products found in the gut, our results confirm the impact – so far largely neglected in the literature – of BS morphological diversity on their bulk aggregation properties. They reveal that the two selected BS display very distinct self-assembly behaviour and interactions with dietary lipids, which correlate with their different interfacial properties [14] and, therefore, support the hypothesis of contrasting roles during the process of fat digestion. More specifically, our results combined together suggest that NaTDC may be more prone to help desorb insoluble lipolysis products from the interface, by

incorporating them into mixed micelles, while NaTC, which has a higher affinity for the interface [14], may be involved in facilitating enzyme adsorption onto fat droplets surfaces.

Future work should focus on investigating the mechanism of liposomes disruption induced by BS, and indeed of other lipidic nanostructures such as emulsions, by monitoring their structural evolution over time, taking advantage of time-resolved scattering experiments and contrast variation. This structural knowledge is key to understanding and thus controlling lipolysis and will help address the issue of excessive lipid uptake and associated cardiometabolic disorders.

CRediT authorship contribution statement

Olivia Pabois: methodology, validation, formal analysis, investigation, writing – original draft, visualisation, project administration; **Robert M. Ziolek, Christian D. Lorenz:** methodology, software, validation, formal analysis, investigation, writing – review and editing, visualisation; **Sylvain Prévost, Najet Mahmoudi, Maximilian W. A. Skoda, Rebbeca J. L. Welbourn, Margarita Valero, Richard D. Harvey, Myriam M.-L. Grundy, Peter J. Wilde:** methodology, writing – review and editing; **Isabelle Grillo, Yuri Gerelli, Cécile A. Dreiss:** conceptualisation, methodology, validation, formal analysis, resources, writing – review and editing, supervision, project administration, funding acquisition.

Declarations of interest

None

Acknowledgments

The authors acknowledge the ILL for the provision of a PhD studentship (OP) and award of beam time on D33 (doi: 10.5291/ILL-DATA.DIR-163), the ESRF for the allocation of beam time on ID02 (test time), ISIS for the award of beam time on SANS2D (doi: 10.5286/ISIS.E.RB1720349) and INTER (doi: 10.5286/ISIS.E.RB1720440), and the Partnership for Soft Condensed Matter (PSCM) for access to sample preparation facilities and the use of the quartz-crystal microbalance with dissipation monitoring and micro-differential scanning calorimeter. OP thanks Nico Carl and Dr Michael Sztucki for performing SAXS measurements, and acknowledges Prof Elliot Gilbert for fruitful discussions on BS bulk aggregation behaviour. This work benefited from the use of the SasView application, originally developed under NSF award DMR-0520547 [99]. RMZ and CDL acknowledge the supportive research environment of the EPSRC Centre for Doctoral Training in Cross-Disciplinary Approaches to Non-Equilibrium Systems (CANES, No. EP/L015854/1). Through CDL's membership within the UK HPC Materials Chemistry Consortium, which is funded by the Office of Science and Technology through the EPSRC High End Computing Programme (Grant No. EP/L000202, EP/R029431), the use of ARCHER, the UK National Supercomputing Service (http://www.archer.ac.uk) and the UK Materials and Molecular Modelling Hub (MMM Hub), which is partially funded by EPSRC

(EP/P020194/1), was made possible for the MD simulations presented in this work. PJW acknowledges the support of the Biotechnology and Biological Sciences Research Council (BBSRC) through the Institute Strategic Programme Food Innovation and Health (BB/R012512/1). SasView contains code developed with funding from the European Union's Horizon 2020 research and innovation programme under the SINE2020 project, grant agreement No 654000. Dr Isabelle Grillo, one of our co-authors and OP's PhD co-supervisor, sadly passed away during the writing-up of this manuscript; we dedicate this to her memory.

References

[1] World Health Organization, Obesity and overweight, (2020). http://www.who.int/mediacentre/factsheets/fs311/en/ (accessed April 18, 2020).

[2] A.F. Hofmann, K.J. Mysels, Bile salts as biological surfactants, Colloids and Surfaces. 30 (1987) 145–173. doi:10.1016/0166-6622(87)80207-X.

[3] J. Maldonado-Valderrama, P. Wilde, A. Macierzanka, A. Mackie, The role of bile salts in digestion, Adv. Colloid Interface Sci. 165 (2011) 36–46. doi:10.1016/j.cis.2010.12.002.

[4] P.J. Wilde, B.S. Chu, Interfacial & colloidal aspects of lipid digestion, Adv. Colloid Interface Sci. 165 (2011) 14–22. doi:10.1016/j.cis.2011.02.004.

[5] B. Borgström, C. Erlanson-Albertsson, T. Wieloch, Pancreatic colipase: chemistry and physiology., J. Lipid Res. 20 (1979) 805–816. http://www.ncbi.nlm.nih.gov/pubmed/385801.

[6] A. Bourbon Freie, F. Ferrato, F. Carrière, M.E. Lowe, Val-407 and Ile-408 in the β5'-loop of pancreatic lipase mediate lipase-colipase interactions in the presence of bile salt micelles, J. Biol. Chem. 281 (2006) 7793–7800. doi:10.1074/jbc.M512984200.

[7] C. Erlanson-Albertsson, The interaction between pancreatic lipase and colipase: a protein-protein interaction regulated by a lipid, FEBS Lett. 162 (1983) 225–229. doi:10.1016/0014-5793(83)80760-1.

[8] S. Labourdenne, O. Brass, M. Ivanova, A. Cagna, R. Verger, Effects of colipase and bile salts on the catalytic activity of human pancreatic lipase. A study using the oil drop tensiometer, Biochemistry. 36 (1997) 3423–3429. doi:10.1021/bi961331k.

[9] A.F. Hofmann, B. Borgström, The intraluminal phase of fat digestion in man: the lipid content of the micellar and oil phases of intestinal content obtained during fat digestion and absorption, J. Clin. Invest. 43 (1964) 247–257. doi:10.1172/JCI104909.

[10] A. Sarkar, A. Ye, H. Singh, On the role of bile salts in the digestion of emulsified lipids, Food Hydrocoll. 60 (2016) 77–84. doi:10.1016/j.foodhyd.2016.03.018.

[11] J. Maldonado-Valderrama, N.C. Woodward, A.P. Gunning, M.J. Ridout, F.A. Husband,

A.R. Mackie, V.J. Morris, P.J. Wilde, Interfacial characterization of β-Lactoglobulin networks: displacement by bile salts, Langmuir. 24 (2008) 6759–6767. doi:10.1021/la800551u.

[12] A. Sarkar, D.S. Horne, H. Singh, Interactions of milk protein-stabilized oil-in-water emulsions with bile salts in a simulated upper intestinal model, Food Hydrocoll. 24 (2010) 142–151. doi:10.1016/j.foodhyd.2009.08.012.

[13] J. Maldonado-Valderrama, J.L. Muros-Cobos, J.A. Holgado-Terriza, M.A. Cabrerizo-Vílchez, Bile salts at the air-water interface: adsorption and desorption, Colloids Surfaces B Biointerfaces. 120 (2014) 176–183. doi:10.1016/j.colsurfb.2014.05.014.

[14] O. Pabois, C.D. Lorenz, R.D. Harvey, I. Grillo, M.M.-L. Grundy, P.J. Wilde, Y. Gerelli, C.A. Dreiss, Molecular insights into the behaviour of bile salts at interfaces: a key to their role in lipid digestion, J. Colloid Interface Sci. 556 (2019) 266–277. doi:10.1016/j.jcis.2019.08.010.

[15] O. Pabois, A. Antoine-Michard, X. Zhao, J. Omar, F. Ahmed, F. Alexis, R.D. Harvey, I. Grillo, Y. Gerelli, M.M.-L. Grundy, B. Bajka, P.J. Wilde, C.A. Dreiss, Interactions of bile salts with a dietary fibre, methylcellulose, and impact on lipolysis, Carbohydr. Polym. 231 (2020) 115741–115751. doi:10.1016/j.carbpol.2019.115741.

[16] R. Parker, N.M. Rigby, M.J. Ridout, A.P. Gunning, P.J. Wilde, The adsorption–desorption behaviour and structure function relationships of bile salts, Soft Matter. 10 (2014) 6457–6466. doi:10.1039/c4sm01093k.

[17] L. Galantini, M.C. di Gregorio, M. Gubitosi, L. Travaglini, J.V. Tato, A. Jover, F. Meijide, V.H. Soto Tellini, N. V. Pavel, Bile salts and derivatives: rigid unconventional amphiphiles as dispersants, carriers and superstructure building blocks, Curr. Opin. Colloid Interface Sci. 20 (2015) 170–182. doi:10.1016/j.cocis.2015.08.004.

[18] S.R. Euston, Molecular simulation of biosurfactants with relevance to food systems, Curr. Opin. Colloid Interface Sci. 28 (2017) 110–119. doi:10.1016/j.cocis.2017.04.002.

[19] D. Madenci, S.U. Egelhaaf, Self-assembly in aqueous bile salt solutions, Curr. Opin. Colloid Interface Sci. 15 (2010) 109–115. doi:10.1016/j.cocis.2009.11.010.

[20] M.C. Carey, Micelle formation by bile salts, Arch. Intern. Med. 130 (1972) 506–527. doi:10.1001/archinte.1972.03650040040005.

[21] L.B. Pártay, P. Jedlovszky, M. Sega, Molecular aggregates in aqueous solutions of bile acid salts. Molecular dynamics simulation study, J. Phys. Chem. B. 111 (2007) 9886–9896. doi:10.1021/jp072974k.

[22] A. Vila Verde, D. Frenkel, Kinetics of formation of bile salt micelles from coarse-grained Langevin dynamics simulations, Soft Matter. 12 (2016) 5172–5179. doi:10.1039/C6SM00763E.

[23] F. Mustan, A. Ivanova, G. Madjarova, S. Tcholakova, N. Denkov, Molecular dynamics simulation of the aggregation patterns in aqueous solutions of bile salts at physiological conditions, J. Phys. Chem. B. 119 (2015) 15631–15643. doi:10.1021/acs.jpcb.5b07063.

[24] N.A. Mazer, M.C. Carey, R.F. Kwasnick, G.B. Benedek, Quasielastic light scattering studies of aqueous biliary lipid systems. Size, shape, and thermodynamics of bile salt micelles, Biochemistry. 18 (1979) 3064–3075. doi:10.1021/bi00581a024.

[25] L.B. Pártay, M. Sega, P. Jedlovszky, Morphology of bile salt micelles as studied by computer simulation methods, Langmuir. 23 (2007) 12322–12328. doi:10.1021/la701749u.

[26] A.J. Clulow, A. Parrow, A. Hawley, J. Khan, A.C. Pham, P. Larsson, C.A.S. Bergström, B.J. Boyd, Characterization of solubilizing nanoaggregates present in different versions of simulated intestinal fluid, J. Phys. Chem. B. 121 (2017) 10869–10881. doi:10.1021/acs.jpcb.7b08622.

[27] J. Santhanalakshmi, G.S. Lakshmi, V.K. Aswal, P.S. Goyal, Small-angle neutron scattering study of sodium cholate and sodium deoxycholate interacting micelles in aqueous medium, J. Chem. Sci. 113 (2001) 55–62. doi:10.1007/BF02708552.

[28] D.B. Warren, D.K. Chalmers, K. Hutchison, W. Dang, C.W. Pouton, Molecular dynamics simulations of spontaneous bile salt aggregation, Colloids Surfaces A Physicochem. Eng. Asp. 280 (2006) 182–193. doi:10.1016/j.colsurfa.2006.02.009.

[29] G. Mangiapia, G. D'Errico, F. Capuano, O. Ortona, R.K. Heenan, L. Paduano, R. Sartorio,

On the interpretation of transport properties of sodium cholate and sodium deoxycholate in binary and ternary aqueous mixtures, Phys. Chem. Chem. Phys. 13 (2011) 15906–15917. doi:10.1039/c1cp20922a.

[30] S. Cozzolino, L. Galantini, C. Leggio, N.V. Pavel, Correlation between small-angle X-ray scattering spectra and apparent diffusion coefficients in the study of structure and interaction of sodium taurodeoxycholate micelles, J. Phys. Chem. B. 109 (2005) 6111–6120. doi:10.1021/jp044540k.

[31] A.A. D'Archivio, L. Galantini, A. Panatta, E. Tettamanti, On the growth and shape of sodium taurodeoxycholate micellar aggregates: a spin-label and quasielastic light scattering investigation, J. Chem. Phys. 120 (2004) 4800–4807. doi:10.1063/1.1645513.

[32] F. Lopez, J. Samseth, K. Mortensen, E. Rosenqvist, J. Rouch, Micro- and macrostructural studies of sodium deoxycholate micellar complexes in aqueous solutions, Langmuir. 12 (1996) 6188–6196. doi:10.1021/la960006v.

[33] H. Matsuoka, J.P. Kratohvil, N. Ise, Small-angle X-ray scattering from solutions of bile salts: sodium taurodeoxycholate in aqueous electrolyte solutions, J. Colloid Interface Sci. 118 (1987) 387–396. doi:10.1016/0021-9797(87)90474-7.

[34] S. Cozzolino, L. Galantini, E. Giglio, S. Hoffmann, C. Leggio, N.V. Pavel, Structure of sodium glycodeoxycholate micellar aggregates from small-angle X-ray scattering and light-scattering techniques, J. Phys. Chem. B. 110 (2006) 12351–12359. doi:10.1021/jp060712x.

[35] H. Kawamura, Y. Murata, T. Yamaguchi, H. Igimi, M. Tanaka, G. Sugihara, J.P. Kratohvil, Spin-label studies of bile salt micelles, J. Phys. Chem. 93 (1989) 3321–3326. doi:10.1021/j100345a087.

[36] A.R. Campanelli, S. Candeloro De Sanctis, E. Giglio, N. Viorel Pavel, C. Quagliata, From crystal to micelle: a new approach to the micellar structure, J. Incl. Phenom. Mol. Recognit. Chem. 7 (1989) 391–400. doi:10.1007/BF01079774.

[37] E. Bottari, A.A. D'Archivio, M.R. Festa, L. Galantini, E. Giglio, Structure and composition of sodium taurocholate micellar aggregates, Langmuir. 15 (1999) 2996–2998. doi:10.1021/la9809630.

[38] L. Galantini, E. Giglio, N.V. Pavel, F. Punzo, QELS and X-ray study of two dihydroxy bile salt aqueous solutions, Colloids Surfaces A Physicochem. Eng. Asp. 248 (2004) 79–84. doi:10.1016/j.colsurfa.2004.06.044.

[39] D.M. Small, M.C. Bourgès, D.G. Dervichian, The biophysics of lipidic associations. I. The ternary systems lecithin-bile salt-water, Biochim. Biophys. Acta. 125 (1966) 563–580. doi:10.1016/0005-2760(66)90044-0.

[40] J. Gustafsson, T. Nylander, M. Almgren, H. Ljusberg-Wahren, Phase behavior and aggregate structure in aqueous mixtures of sodium cholate and glycerol monooleate, J. Colloid Interface Sci. 211 (1999) 326–335. doi:10.1006/jcis.1998.5996.

[41] M. Svaerd, P. Schurtenberger, K. Fontell, B. Joensson, B. Lindman, Micelles, vesicles, and liquid crystals in the monoolein-sodium taurocholate-water system: phase behavior, NMR, self-diffusion, and quasi-elastic light scattering studies, J. Phys. Chem. 92 (1988) 2261–2270. doi:10.1021/j100319a034.

[42] P. Garidel, A. Hildebrand, K. Knauf, A. Blume, Membranolytic activity of bile salts: influence of biological membrane properties and composition, Molecules. 12 (2007) 2292–2326. doi:10.3390/12102292.

[43] A. Hildebrand, K. Beyer, R. Neubert, P. Garidel, A. Blume, Temperature dependence of the interaction of cholate and deoxycholate with fluid model membranes and their solubilization into mixed micelles, Colloids Surfaces B Biointerfaces. 32 (2003) 335–351. doi:10.1016/j.colsurfb.2003.08.001.

[44] A. Hildebrand, R. Neubert, P. Garidel, A. Blume, Bile salt induced solubilization of synthetic phosphatidylcholine vesicles studied by isothermal titration calorimetry, Langmuir. 18 (2002) 2836–2847. doi:10.1021/la011421c.

[45] L. Forte, K. Andrieux, G. Keller, C. Grabielle-Madelmont, S. Lesieur, M. Paternostre, M. Ollivon, C. Bourgaux, P. Lesieur, Sodium taurocholate-induced lamellar-micellar phase transitions of DPPC, J. Therm. Anal. Calorim. 51 (1998) 773–782. doi:10.1007/BF03341454.

[46] G.A. Kossena, B.J. Boyd, C.J.H. Porter, W.N. Charman, Separation and characterization of the colloidal phases produced on digestion of common formulation lipids and

assessment of their impact on the apparent solubility of selected poorly water-soluble drugs, J. Pharm. Sci. 92 (2003) 634–648. doi:10.1002/jps.10329.

[47] M.A. Long, E.W. Kaler, S.P. Lee, Structural characterization of the micelle-vesicle transition in lecithin-bile salt solutions, Biophys. J. 67 (1994) 1733–1742. doi:10.1016/S0006-3495(94)80647-2.

[48] R.P. Hjelm, P. Thiyagarajan, H. Alkan, A small-angle neutron scattering study of the effects of dilution on particle morphology in mixtures of glycocholate and lecithin, J. Appl. Crystallogr. 21 (1988) 858–863. doi:10.1107/S002188988800531X.

[49] P. Schurtenberger, M. Svärd, E. Wehrli, B. Lindman, Vesicle formation in aqueous solutions of bile salt and monoacylglycerol, Biochim. Biophys. Acta. 882 (1986) 465–468. doi:10.1016/0304-4165(86)90271-0.

[50] R.P. Hjelm, C. Schteingart, A.F. Hofmann, D.S. Sivia, Form and structure of self-assembling particles in monoolein-bile salt mixtures, J. Phys. Chem. 99 (1995) 16395–16406. doi:10.1021/j100044a030.

[51] R.P. Hjelm, P. Thiyagarajan, H. Alkan-Onyuksel, Organization of phosphatidylcholine and bile salt in rodlike mixed micelles, J. Phys. Chem. 96 (1992) 8653–8661. doi:10.1021/j100200a080.

[52] D. Madenci, A. Salonen, P. Schurtenberger, J.S. Pedersen, S.U. Egelhaaf, Simple model for the growth behaviour of mixed lecithin–bile salt micelles, Phys. Chem. Chem. Phys. 13 (2011) 3171–3178. doi:10.1039/C0CP01700K.

[53] W.A. Birru, D.B. Warren, A. Ibrahim, H.D. Williams, H. Benameur, C.J.H. Porter, D.K. Chalmers, C.W. Pouton, Digestion of phospholipids after secretion of bile into the duodenum changes the phase behavior of bile components, Mol. Pharm. 11 (2014) 2825–2834. doi:10.1021/mp500193g.

[54] A. Walter, P.K. Vinson, A. Kaplun, Y. Talmon, Intermediate structures in the cholate-phosphatidylcholine vesicle-micelle transition, Biophys. J. 60 (1991) 1315–1325. doi:10.1016/S0006-3495(91)82169-5.

[55] M.A. Kiselev, M. Janich, A. Hildebrand, P. Strunz, R.H.H. Neubert, D. Lombardo,

Structural transition in aqueous lipid/bile salt [DPPC/NaDC] supramolecular aggregates: SANS and DLS study, Chem. Phys. 424 (2013) 93–99. doi:10.1016/j.chemphys.2013.05.014.

[56] K. Andrieux, L. Forte, S. Lesieur, M. Paternostre, M. Ollivon, C. Grabielle-Madelmont, Solubilisation of dipalmitoylphosphatidylcholine bilayers by sodium taurocholate: a model to study the stability of liposomes in the gastrointestinal tract and their mechanism of interaction with a model bile salt, Eur. J. Pharm. Biopharm. 71 (2009) 346–355. doi:10.1016/j.ejpb.2008.09.004.

[57] K. Kalyanasundaram, J.K. Thomas, Environmental effects on vibronic band intensities in pyrene monomer fluorescence and their application in studies of micellar systems, J. Am. Chem. Soc. 99 (1977) 2039–2044. doi:10.1021/ja00449a004.

[58] M. Buchweitz, P.A. Kroon, G.T. Rich, P.J. Wilde, Quercetin solubilisation in bile salts: a comparison with sodium dodecyl sulphate, Food Chem. 211 (2016) 356–364. doi:10.1016/j.foodchem.2016.05.034.

[59] J. Webster, S. Holt, R. Dalgliesh, INTER the chemical interfaces reflectometer on target station 2 at ISIS, Phys. B. 385–386 (2006) 1164–1166. doi:10.1016/j.physb.2006.05.400.

[60] J.A. Hamilton, Interactions of triglycerides with phospholipids: incorporation into the bilayer structure and formation of emulsions, Biochemistry. 28 (1989) 2514–2520. doi:10.1021/bi00432a025.

[61] R.J. Deckelbaum, J.A. Hamilton, A. Moser, G. Bengtsson-Olivecrona, E. Butbul, Y.A. Carpentier, A. Gutman, T. Olivecrona, Medium-chain versus long-chain triacylglycerol emulsion hydrolysis by lipoprotein lipase and hepatic lipase: implications for the mechanisms of lipase action, Biochemistry. 29 (1990) 1136–1142. doi:10.1021/bi00457a006.

[62] J.A. Hamilton, D.M. Small, Solubilization and localization of triolein in phosphatidylcholine bilayers: a 13C NMR study., Proc. Natl. Acad. Sci. 78 (1981) 6878–6882. doi:10.1073/pnas.78.11.6878.

[63] C. Rojas, T. Olivecrona, G. Bengtsson-Olivecrona, Comparison of the action of lipoprotein lipase on triacylglycerols and phospholipids when presented in mixed

liposomes or in emulsion droplets, Eur. J. Biochem. 197 (1991) 315–321. doi:10.1111/j.1432-1033.1991.tb15913.x.

[64] D. Guard-Friar, C.-H. Chen, A.S. Engle, Deuterium isotope effect on the stability of molecules: phospholipids, J. Phys. Chem. 89 (1985) 1810–1813. doi:10.1021/j100255a054.

[65] G. Bryant, M.B. Taylor, T.A. Darwish, A.M. Krause-Heuer, B. Kent, C.J. Garvey, Effect of deuteration on the phase behaviour and structure of lamellar phases of phosphatidylcholines – Deuterated lipids as proxies for the physical properties of native bilayers, Colloids Surfaces B Biointerfaces. 177 (2019) 196–203. doi:10.1016/j.colsurfb.2019.01.040.

[66] D. Madenci, Study of the aggregation behaviour of egg yolk lecithin/bile salt mixtures by increasing the ionic strength, The University of Edinburgh, 2009. http://hdl.handle.net/1842/4918.

[67] P. Van Vaerenbergh, J. Léonardon, M. Sztucki, P. Boesecke, J. Gorini, L. Claustre, F. Sever, J. Morse, T. Narayanan, An upgrade beamline for combined wide, small and ultra small-angle x-ray scattering at the ESRF, in: AIP Conf. Proc., 2016: pp. 030034-1-030034–4. doi:10.1063/1.4952857.

[68] R.K. Heenan, S.E. Rogers, D. Turner, A.E. Terry, J. Treadgold, S.M. King, Small angle neutron scattering using Sans2d, Neutron News. 22 (2011) 19–21. doi:10.1080/10448632.2011.569531.

[69] C.D. Dewhurst, I. Grillo, D. Honecker, M. Bonnaud, M. Jacques, C. Amrouni, A. Perillo-Marcone, G. Manzin, R. Cubitt, The small-angle neutron scattering instrument D33 at the Institut Laue-Langevin, J. Appl. Crystallogr. 49 (2016) 1–14. doi:10.1107/S1600576715021792.

[70] S. Nosé, A molecular dynamics method for simulations in the canonical ensemble, Mol. Phys. 52 (1984) 255–268. doi:10.1080/00268978400101201.

[71] W.G. Hoover, Canonical dynamics: equilibrium phase-space distributions, Phys. Rev. A. 31 (1985) 1695–1697. doi:10.1103/PhysRevA.31.1695.

[72] M. Parrinello, A. Rahman, Polymorphic transitions in single crystals: a new molecular dynamics method, J. Appl. Phys. 52 (1981) 7182–7190. doi:10.1063/1.328693.

[73] D. Van Der Spoel, E. Lindahl, B. Hess, G. Groenhof, A.E. Mark, H.J.C. Berendsen, GROMACS: fast, flexible, and free, J. Comput. Chem. 26 (2005) 1701–1718. doi:10.1002/jcc.20291.

[74] M.J. Abraham, T. Murtola, R. Schulz, S. Páll, J.C. Smith, B. Hess, E. Lindahl, GROMACS: high performance molecular simulations through multi-level parallelism from laptops to supercomputers, SoftwareX. 1–2 (2015) 19–25. doi:10.1016/j.softx.2015.06.001.

[75] K. Vanommeslaeghe, E. Hatcher, C. Acharya, S. Kundu, S. Zhong, J. Shim, E. Darian, O. Guvench, P. Lopes, I. Vorobyov, A.D. Mackerell Jr., CHARMM general force field: a force field for drug-like molecules compatible with the CHARMM all-atom additive biological force fields, J. Comput. Chem. 31 (2010) 671–690. doi:10.1002/jcc.21367.

[76] W.L. Jorgensen, J. Chandrasekhar, J.D. Madura, R.W. Impey, M.L. Klein, Comparison of simple potential functions for simulating liquid water, J. Chem. Phys. 79 (1983) 926–935. doi:10.1063/1.445869.

[77] W.E. Reiher, Theoretical studies of hydrogen bonding, Harvard University, 1985.

[78] B. Hess, H. Bekker, H.J.C. Berendsen, J.G.E.M. Fraaije, LINCS: a linear constraint solver for molecular simulations, J. Comput. Chem. 18 (1997) 1463–1472. doi:10.1002/(SICI)1096-987X(199709)18:12<1463::AID-JCC4>3.0.CO;2-H.

[79] N. Michaud-Agrawal, E.J. Denning, T.B. Woolf, O. Beckstein, MDAnalysis: a toolkit for the analysis of molecular dynamics simulations, J. Comput. Chem. 32 (2011) 2319–2327. doi:10.1002/jcc.21787.

[80] R.J. Gowers, M. Linke, J. Barnoud, T.J.E. Reddy, M.N. Melo, S.L. Seyler, J. Domański, D.L. Dotson, S. Buchoux, I.M. Kenney, O. Beckstein, MDAnalysis: a python package for the rapid analysis of molecular dynamics simulations, in: S. Benthall, S. Rostrup (Eds.), Proc. 15th Python Sci. Conf., 2016: pp. 98–105. doi:10.25080/Majora-629e541a-00e.

[81] A.A. Hagberg, D.A. Schult, P.J. Swart, Exploring network structure, dynamics, and function using NetworkX, in: G. Varoquaux, T. Vaught, J. Millman (Eds.), Proc. 7th

Python Sci. Conf., 2008: pp. 11–16.

[82] S. Hashimoto, J.K. Thomas, Photophysical studies of pyrene in micellar sodium taurocholate at high salt concentrations, J. Colloid Interface Sci. 102 (1984) 152–163. doi:10.1016/0021-9797(84)90209-1.

[83] G. Li, L.B. McGown, Model for bile salt micellization and solubilization from studies of a “polydisperse” array of fluorescent probes and molecular modeling, J. Phys. Chem. 98 (1994) 13711–13719. doi:10.1021/j100102a043.

[84] K. Matsuoka, M. Maeda, Y. Moroi, Micelle formation of sodium glyco- and taurocholates and sodium glyco- and taurodeoxycholates and solubilization of cholesterol into their micelles, Colloids Surfaces B Biointerfaces. 32 (2003) 87–95. doi:10.1016/S0927-7765(03)00148-6.

[85] B. Mukherjee, A.A. Dar, P.A. Bhat, S.P. Moulik, A.R. Das, Micellization and adsorption behaviour of bile salt systems, RSC Adv. 6 (2016) 1769–1781. doi:10.1039/C5RA20909A.

[86] J.W. Brady, L. Tavagnacco, L. Ehrlich, M. Chen, U. Schnupf, M.E. Himmel, M.-L. Saboungi, A. Cesàro, Weakly hydrated surfaces and the binding interactions of small biological solutes, Eur. Biophys. J. 41 (2012) 369–377. doi:10.1007/s00249-011-0776-2.

[87] S. Phan, S. Salentinig, E. Gilbert, T.A. Darwish, A. Hawley, R. Nixon-Luke, G. Bryant, B.J. Boyd, Disposition and crystallization of saturated fatty acid in mixed micelles of relevance to lipid digestion, J. Colloid Interface Sci. 449 (2015) 160–166. doi:10.1016/j.jcis.2014.11.026.

[88] T.A. Harroun, J. Katsaras, S.R. Wassall, Cholesterol is found to reside in the center of a polyunsaturated lipid membrane, Biochemistry. 47 (2008) 7090–7096. doi:10.1021/bi800123b.

[89] H. Khandelia, L. Duelund, K.I. Pakkanen, J.H. Ipsen, Triglyceride blisters in lipid bilayers: implications for lipid droplet biogenesis and the mobile lipid signal in cancer cell membranes, PLoS One. 5 (2010) 1–8. doi:10.1371/journal.pone.0012811.

[90] Y. Gerelli, M.T. Di Bari, A. Deriu, L. Cantù, P. Colombo, C. Como, S. Motta, F. Sonvico, R. May, Structure and organization of phospholipid/polysaccharide nanoparticles, J. Phys.

Condens. Matter. 20 (2008) 104211–104218. doi:10.1088/0953-8984/20/10/104211.

[91] A. Hildebrand, K. Beyer, R. Neubert, P. Garidel, A. Blume, Solubilization of negatively charged DPPC/DPPG liposomes by bile salts, J. Colloid Interface Sci. 279 (2004) 559–571. doi:10.1016/j.jcis.2004.06.085.

[92] H.-J. Mögel, M. Wahab, R. Schmidt, P. Schiller, Computer simulation of the solubilization of liposomes by bile salts, Chem. Lett. 41 (2012) 1066–1068. doi:10.1246/cl.2012.1066.

[93] M. Haustein, P. Schiller, M. Wahab, H.-J. Mögel, Computer simulations of the formation of bile salt micelles and bile salt/DPPC mixed micelles in aqueous solutions, J. Solution Chem. 43 (2014) 1755–1770. doi:10.1007/s10953-014-0239-3.

[94] T.M. McCoy, J.B. Marlow, A.J. Armstrong, A.J. Clulow, C.J. Garvey, M. Manohar, T.A. Darwish, B.J. Boyd, A.F. Routh, R.F. Tabor, Spontaneous Self-Assembly of Thermoresponsive Vesicles Using a Zwitterionic and an Anionic Surfactant, Biomacromolecules. (2020). doi:10.1021/acs.biomac.0c00672.

[95] M.J. Armstrong, M.C. Carey, The hydrophobic-hydrophilic balance of bile salts. Inverse correlation between reverse-phase high performance liquid chromatographic mobilities and micellar cholesterol-solubilizing capacities., J. Lipid Res. 23 (1982) 70–80. http://www.ncbi.nlm.nih.gov/pubmed/7057113.

[96] R.P. Hjelm, C.D. Schteingart, A.F. Hofmann, P. Thiyagarajan, Structure of conjugated bile salt-fatty acid-monoglyceride mixed colloids: studies by small-angle neutron scattering, J. Phys. Chem. B. 104 (2000) 197–211. doi:10.1021/jp992157n.

[97] O. Rezhdo, S. Di Maio, P. Le, K.C. Littrell, R.L. Carrier, S.-H. Chen, Characterization of colloidal structures during intestinal lipolysis using small-angle neutron scattering, J. Colloid Interface Sci. 499 (2017) 189–201. doi:10.1016/j.jcis.2017.03.109.

[98] A.F. Hofmann, The function of bile salts in fat absorption. The solvent properties of dilute micellar solutions of conjugated bile salts., Biochem. J. 89 (1963) 57–68. doi:10.1042/bj0890057.

[99] SasView for small angle scattering analysis, (2018). www.sasview.org (accessed August 22, 2018).